Fock-space relativistic coupled-cluster calculations of two-valence atoms

B. K. Mani and D. Angom

Physical Research Laboratory, Navarangpura-380009, Gujarat, India

(Received 29 September 2010; published 7 January 2011)

We have developed an all-particle Fock-space relativistic coupled-cluster method for two-valence atomic systems. We then describe a scheme to employ the coupled-cluster wave function to calculate atomic properties. Based on these developments we calculate the excitation energies, magnetic hyperfine structure constants, and electric dipole matrix elements of Sr, Ba, and Yb. Furthermore, we calculate the electric quadrupole hyperfine structure constants and the electric dipole matrix elements of Sr^+, Ba^+, and Yb^+. For these we use the one-valence coupled-cluster wave functions obtained as an intermediate in the two-valence calculations. We also calculate the magnetic dipole hyperfine structure constants of Yb^+.

I. INTRODUCTION

Coupled-cluster theory (CCT), first developed in nuclear many-body physics [1,2], is considered one of the best many-body theories. In recent times, it has been used with great success in nuclear [3], atomic [4,5], molecular [6], and condensed matter [7] calculations. A recent review [8] provides a detailed overview of the theory and variations suitable to different classes of many-body systems. An earlier review provides an overview on the application of coupled-cluster theory to various areas of physics [9]. In atoms it is equivalent to incorporating electron correlation effects to all order. It has been used extensively in precision atomic structure and properties calculations. These include atomic electric dipole moments [4,10], parity nonconservation [11], hyperfine structure (HFS) constants [5,12], and electromagnetic transition properties [13,14].

In this paper we report the development and results of relativistic coupled-cluster (CC) atomic calculations for two-valence atoms. For this we employ the Fock-space open-shell CCT [15,16], which is also referred to as valence universal. Based on which the two-valence CC wave operators are calculated using the closed and one-valence wave operators. The necessary developments of these intermediate stages of calculations were reported in our previous works [17,18]. We emphasize that in Ref. [18] we proposed a scheme to calculate properties with CC wave functions to all order. In the present work we implement two-valence Fock-space relativistic CCT with an all-particle valence space. A similar approach was adopted in a previous work on relativistic coupled-cluster calculations of two-valence systems [19]. This is general enough for the precise wave function and properties calculations of the low-lying levels of two-valence systems like the alkaline-earth metal atoms, Yb and Hg. In these systems, the low-lying levels arise from the ns^2, $ns(n-1)d$ and $nsnp$ configurations. We show selecting a model space consisting of these configurations is incomplete but quasicomplete. The advantage of a quasicomplete model space is that it has all the virtues of a complete model space but one can circumvent the divergence associated with *intruder* states [20] in open-shell CCT. The calculations presented in this work are based on coupled-cluster singles and doubles (CCSD) approximation. It was initially formulated for molecular calculations [21] and used in atomic structure calculations to study the excitation energies of Li [22]. Later, the relativistic version was implemented to calculate structure and properties of high Z atoms and ions [5,23,24].

In the present work we apply the method we have developed to calculate the wave functions of alkaline-earth-metal atoms Sr and Ba, and lanthanide atom Yb. All of these atoms are candidates of extremely precise experiments either for application-oriented investigations or to probe fundamental laws of nature. Atomic Sr, which was recently cooled to quantum degeneracy [25], is a strong contender of future optical clocks [26,27]. Experiments on Bose-Einstein statistics violations have used Ba as the target atom [28] and it is an ideal proxy, both for experimental [29] and theoretical [30] studies, of atomic Ra. It is an atom with large parity and time-reversal violation effects [31], and promising candidate for future experiments. Recently, parity violation was detected in Yb [32] and ongoing experiments could lead to unambiguous detection of nuclear anapole [33]. An exotic parity violating nuclear moment, which can be detected only through atomic experiments. There are also proposals to measure atomic electric dipole moment, a signature of parity and time violations, with novel techniques [34,35]. It must be mentioned that several isotopes of Yb have been cooled to degeneracy [36] and could be employed in future precision measurements. Furthermore, atomic Yb in an optical lattice is a candidate of frequency standard [37].

As mentioned before, to obtain the two-valence wave operator, we compute the closed-shell and one-valence wave operators in the intermediate steps. We take advantage of this and use the one-valence wave operator to compute the hyperfine constants of Sr^+, Ba^+, and Yb^+. For the first two ions, we reported the magnetic hyperfine structure constants in our previous paper [18], so we compute only the electric quadrupole HFS constants, whereas for Yb^+ we compute both the magnetic dipole and electric quadrupole HFS constants. In addition, we also compute the electric dipole transitions matrix elements. Like the neutral atoms, all the ions are under experimental investigations for various precision measurements. For example, a single trapped $^{87}Sr^+$ is a suitable frequency standard [38]. There are similar experiments with Yb^+ [39] as an alternative frequency standard. And it is one of the frequency standards in the laboratory measurement of temporal variation of fine structure constant [40]. These are application oriented

precision experiments. The other fascinating prospect is the observation of parity nonconservation in a single ^{137}Ba$^+$ [41].

The paper is divided into seven sections. In Sec. II we give a brief description of many-body perturbation theory (MBPT) for two-valence systems. It provides the minimal description of concepts pertinent to development of two-valence coupled-cluster theory. Section III is a short writeup on closed-shell and one-valence CCT followed by derivation of the two-valence CCT in some detail. These are in the context of complete model space. Incomplete model space CCT is explained in Sec. IV and atomic Yb is discussed as an example. Calculation of properties, HFS constants, and electric dipole transition, with CC wave functions is the topic of Sec. V. In Sec. VI, the important details of implementing two-valence CCT is explained, however, with emphasis on physics. Finally, results and discussions are reported in Sec. VII. In the paper, all the calculations and mathematical expressions are in atomic units ($e = \hbar = m_e = 4\pi\epsilon_0 = 1$).

II. MBPT FOR TWO-VALENCE ATOMS

Relativistic effects are the key to obtain accurate results in the structure and properties calculations of high Z atoms with $z\alpha \sim 1$. The Dirac-Coulomb Hamiltonian $H^{\rm DC}$ is an approximate but an appropriate Hamiltonian to describe the properties of such atoms. For an atom with N electrons,

$$H^{\rm DC} = \sum_{i=1}^{N} [c\boldsymbol{\alpha}_i \cdot \boldsymbol{p}_i + (\beta - 1)c^2 - V_N(r_i)] + \sum_{i<j} \frac{1}{r_{ij}}, \quad (1)$$

where $\boldsymbol{\alpha}_i$ and β are the Dirac matrices, $\boldsymbol{p}$ is the linear momentum, $V_N(r)$ is the nuclear Coulomb potential, and the last term is the electron-electron Coulomb interactions. It satisfies, in the case of two-valence atoms, the eigenvalue equation,

$$H^{\rm DC}|\Psi_{vw}\rangle = E_{vw}|\Psi_{vw}\rangle, \quad (2)$$

where indexes v and w represent the valence orbitals, $|\Psi_{vw}\rangle$ is the exact wave function, and E_{vw} is the exact energy of the two-valence atomic system. In MBPT, the total Hamiltonian, in Eq. (1), is separated into two parts: $H_0 = \sum_i [c\boldsymbol{\alpha}_i \cdot \boldsymbol{p}_i + (\beta_i - 1)c^2 - V_N r_i + u(\mathbf{r}_i)]$, the unperturbed or exactly solvable part, and $V = \sum_{i<j}^{N} \frac{1}{\mathbf{r}_{ij}} - \sum_i u(\mathbf{r}_i)$, the perturbation, referred to as the residual Coulomb interaction. The unperturbed eigenfunctions $|\Phi_{vw}\rangle$ are the solution of the Dirac-Fock equation,

$$H_0|\Phi_{vw}\rangle = E_{vw}^{(0)}|\Phi_{vw}\rangle, \quad (3)$$

where $|\Phi_{vw}\rangle$ are the antysymmetrized many-electron wave functions. Formally, in operator notations, these are generated from the closed-shell reference state $|\Phi_0\rangle$ as $|\Phi_{vw}\rangle = a_v^\dagger a_w^\dagger |\Phi_0\rangle$, and the eigenvalue $E_{vw}^{(0)}$ is the sum of the single electron energies. These are the basic starting points common to atomic MBPT and coupled-cluster theory. The two theories share a common thread until the generalized Bloch equation [42], discussed in the next section, but is significantly different from there on.

A. Generalized Bloch equation

In this section, and others as well, we provide the basic equations and necessary definitions essential to a lucid description of the method we have developed and used. For detailed descriptions appropriate references are provided. In MBPT, the Hilbert space of the eigenfunctions $|\Phi_{vw}\rangle$ is separated into two submanifolds: model space (P), comprising the eigenfunctions which are the best approximation to the exact eigenfunctions of interest and the remaining spans the orthogonal space (Q). In the single reference theory, the exact state $|\Psi_{vw}\rangle$ and model state $|\Phi_{vw}\rangle$ are related as

$$|\Psi_{vw}\rangle = \Omega|\Phi_{vw}\rangle, \quad (4)$$

where, Ω is the wave operator and is the solution of the generalized Bloch equation,

$$[\Omega, H_0]P = (V\Omega - \Omega P V\Omega)P. \quad (5)$$

Detailed exposition of the equation and relevant derivations are given Refs. [42,43]. Here, intermediate normalization,

$$|\Phi_{vw}\rangle = P\Omega|\Phi_{vw}\rangle, \quad (6)$$

is a necessary condition to obtain the generalized Bloch equation. In singles and doubles approximation, an often used and well-tested method in atomic calculations, the wave operator is

$$\Omega = 1 + x_a^p a_p^\dagger a_a + x_v^p a_p^\dagger a_v + \frac{1}{2} x_{ab}^{pq} a_p^\dagger a_q^\dagger a_b a_a$$
$$+ x_{av}^{pq} a_p^\dagger a_q^\dagger a_v a_a + \frac{1}{2} x_{vw}^{pq} a_p^\dagger a_q^\dagger a_w a_v, \quad (7)$$

where $ab\cdots (pq\cdots)$ denote core (virtual) orbitals and $x_{\cdots}^{\cdots}$ are the excitation amplitudes. This definition is crucial to our later discussions on the Fock space coupled cluster in complete model space (CMS). Unlike the closed-shell atoms, the model wave functions are not known in the case of open-shell systems. These are obtained by diagonalizing the effective Hamiltonian ($H_{\rm eff}$) matrix, calculated within the P submanifold. Once the model wave function is obtained, the exact energy is the expectation value of $H_{\rm eff}$, as it satisfies the eigenvalue equation,

$$H_{\rm eff}|\Phi_{vw}\rangle = E_{vw}|\Phi_{vw}\rangle. \quad (8)$$

The effective Hamiltonian, in Eq. (8), is expressed as

$$H_{\rm eff} = P H_0 P + P V \Omega P, \quad (9)$$

where H_0 and V, as defined earlier, are the zeroth-order Hamiltonian and the residual Coulomb interaction, respectively. The first term in Eq. (9) is the leading contribution, $E_{vw}^{(0)}$, to the total energy E_{vw}. And the second term, with the wave operator Ω, is the correction to $E_{vw}^{(0)}$ referred to as correlation energy.

B. First- and second-order effective Hamiltonians

From Eq. (8), the first-order correction to energy is the expectation value of the first-order effective Hamiltonian,

$$H_{\rm eff}^{(1)} = PVP = P(V_0 + V_1 + V_2)P, \quad (10)$$

where V_0 is the contribution from the closed-shell part and represented by the closed diagrams with no free lines at the vertexes. We exclude this term while calculating the excitation

energies as it is common to all the diagonal elements of the H_{eff} matrix. It effectively shifts all the energy levels equally and does not account for the energy level splitting. The one- and two-body terms, V_1 and V_2, have contributions from the open-shell part only. The contributing diagrams are the closed diagrams with free valence lines at the vertices. The one-body term V_1 also contributes to the diagonal elements only and hence does not contribute to the energy level splitting. From Eq. (10), $H_{\text{eff}}^{(1)}$ is reduced to the form,

$$H_{\text{eff}}^{(1)} = P V_2 P. \tag{11}$$

This term contributes through a closed diagram with one pair of valence lines at each vertex shown in Fig. 2(a).

From Eq. (9), the second-order effective Hamiltonian,

$$H_{\text{eff}}^{(2)} = P V \Omega^{(1)} P = P(V_1 + V_2)\big(\Omega_1^{(1)} + \Omega_2^{(1)}\big) P, \tag{12}$$

where the superscript in the wave operator represents the order of the perturbation. Contributing diagrams are closed diagrams with valence orbitals as free lines at the vertexes. Detailed description of the relativistic second MBPT of two-valence systems is given in Ref. [44]. The terms involving V_1 are zero if Dirac-Fock orbitals are used in the calculations. The expression of $H_{\text{eff}}^{(2)}$ is

$$H_{\text{eff}}^{(2)} = P \overset{\frown}{V_2 \Omega_2^{(1)}} P, \tag{13}$$

where $\{\overset{\frown}{A \cdots B}\}$ represents contraction between two operators A and B.

The diagrams of $H_{\text{eff}}^{(2)}$, in Eq. (13), are separated into two categories. The diagrams with one pair of free lines as the valence orbitals, shown in Fig. 1, constitute the one-body effective operator. And the diagrams with two pair of free lines as the valence orbitals, shown in Fig. 2, form the two-body effective operator. It must be mentioned that a previous work reported the third-ordered relativistic MBPT calculations of two-valence systems beryllium and magnesium iso-electronic sequences [45].

C. H_{eff} matrix elements with jj coupled states

In our scheme of calculations, we first evaluate the diagrams arising from Eqs. (11) and (13), Figs. 1 and 2, using uncoupled states. And we then store these as the effective one- and two-body operators. Later we use these effective operators to generate the matrix elements with respect to the jj coupled states. For two nonequivalent electrons the jj coupled
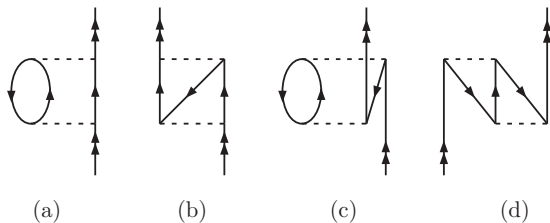

FIG. 1. One-body diagrams arising from the second-order effective Hamiltonian $H_{\text{eff}}^{(2)}$.
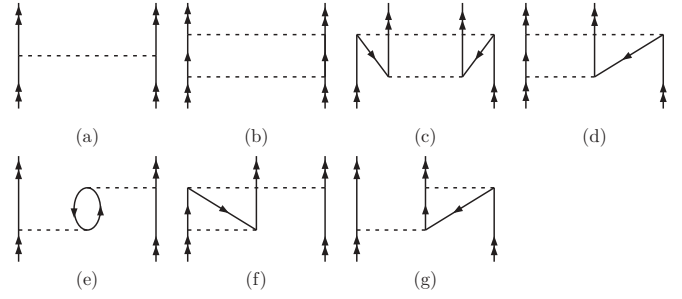

FIG. 2. The two-body diagram (a) arises from the first-order effective Hamiltonian $H_{\text{eff}}^{(1)}$. The remaining two-body diagrams, from (b)–(g), contribute to the second-order effective Hamiltonian $H_{\text{eff}}^{(2)}$.

antysymmetrized state may be expressed, in terms of the total angular momentum J state, as

$$
\begin{aligned}
&|\{\gamma_v j_v m_v \gamma_w j_w m_w\} J M\rangle \\
&= \frac{1}{\sqrt{2}}[|(\gamma_v j_v m_v \gamma_w j_w m_w) J M\rangle \\
&\quad + (-1)^{j_v + j_w + J} |(\gamma_w j_w m_w \gamma_v j_v m_v) J M\rangle],
\end{aligned}
\tag{14}
$$

where j_v and j_w are the total angular momenta of the single electron states $|\phi_v\rangle$ and $|\phi_w\rangle$, respectively, γ_v and γ_w are additional quantum numbers to specify the states uniquely. And m_v and m_w are the corresponding magnetic quantum numbers. Similarly, J and M are the total angular momentum of the coupled state and magnetic quantum number, respectively. The matrix element of a two-body operator then consists of four terms, two direct and two exchange, with the normalization factor $1/2$.

To evaluate the two-body matrix element, for example, the coulomb interaction shown Fig. 2(a). The direct matrix element is of the form,

$$
\begin{aligned}
&\langle (\gamma_v j_v m_v \gamma_w j_w m_w) J M | \frac{1}{r_{12}} | (\gamma_x j_x m_x \gamma_y j_y m_y) J' M'\rangle \\
&= \sum_k (-1)^{j_x + j_w + J + k} \delta(J, J') \delta(M, M') \begin{Bmatrix} j_x & j_x & k \\ j_y & j_w & J \end{Bmatrix} \\
&\quad \times \langle \gamma_v j_v || \mathbf{C}^k || \gamma_x j_x\rangle \langle \gamma_w j_w || \mathbf{C}^k || \gamma_y j_y\rangle R^k,
\end{aligned}
\tag{15}
$$

where x and y represent valence orbitals, R^k is the radial integral, and $\mathbf{C}^k$ is the spherical tensor operator. For matrix elements in Eq. (15) to be nonzero the states should have the same parity and J. The relation in Eq. (15) holds true for the matrix elements of the other two-body diagrams [Figs. 2(b)–2(g)]. In this case the multipole k and the radial integral arise from the combination of two orders of residual Coulomb interactions.

Similarly, the matrix element of the one-body operator of rank k, with respect to the jj coupled state is

$$
\begin{aligned}
&\langle (\gamma_v j_v \gamma_w j_w) J M | \mathbf{F}^k(1) | (\gamma_x j_x \gamma_y j_y) J' M'\rangle \\
&= \delta(\gamma_w, \gamma_y) \delta(j_w, j_y) (-1)^{J - M} (-1)^{j_v + j_y + J' + k} [J, J']^{1/2}, \\
&\quad \times \begin{pmatrix} J & k & J' \\ -M & 0 & M \end{pmatrix} \begin{Bmatrix} j_v & j_x & k \\ J' & J & j_w \end{Bmatrix} \langle \gamma_v j_v || \mathbf{f}^k || \gamma_x j_x\rangle.
\end{aligned}
\tag{16}
$$

This is a very general expression and applicable to one-body operator of any rank k. In our calculations, however, we use $k = 0$ as the one-body effective operator is scalar.

III. FOCK-SPACE CCT: COMPLETE MODEL SPACE

A model space is complete if it consists of all the configurations formed by accommodating the valence electrons among the valence shells in all possible combinations. A remarkable consequence of choosing CMS in Fock-space coupled cluster is that the excitation operators $x^{\cdots}_{\cdots}$ are common to all the determinants in the model space. Furthermore, $x^{\cdots}_{\cdots}$ uniquely separates into internal and external sectors. The external excitations contribute to Ω and projects a model function to the complementary space, whereas, internal excitations connect one model function to another model function and occur in the definition of H_{eff}. As we shall explore later, in the context of incomplete model space (IMS), such a neat separation is specific to CMS and another class of model space referred to as quasicomplete [43]. Validity of linked cluster theorem, one basic condition for any legitimate many-body theory, is assured in CMS.

The CMS, though endowed with several desirable properties, has one serious shortcoming for systems with two or more valence electrons. It inevitably encounters *intruder* states [20] and the outcome is severe convergence problems. This is the manifestation of model states with high energies that lies within the energy domain of the orthogonal space. In other words, in CMS when all possible configurations are considered, the model and complementary space are no longer energetically well separated. The occurrence of vanishing energy denominators is then a distinct possibility. Indeed, we invariably encounter *intruder* states in all our two-valence calculations with CMS. Its presence is the rule rather than the exception.

For a better description of the CMS and intruder states let us consider a specific example, the low-lying levels of Yb atom. Configurations and terms of the ground and first few excited states important in precision spectroscopy are $6s^2(^1S_0)$, $6s6p(^3P_J)$, $5d6s(^3D_J)$, and $6s6p(^1P_1)$. The $6s$, $6p$, and $5d$ are then the obvious choice of valence shells. CMS of the system then consists of the configurations: $6s^2$, $6s6p$, $5d6s$, $5d6p$, $6p^2$, and $5d^2$ and all the other configurations are in the complementary space. As shown in Fig. 3, the levels from the orthogonal space $6p7p(^3P_J)$, $6s7s(^3S_1)$, and $6s7s(^1S_0)$ lie within the model space. With several orthogonal functions within the energy domain of model functions, CMS-based CCT calculations of Yb are likely to face with intruder-state-related divergences. Indeed, we do encounter divergences which, on careful analysis, can be attributed to the intruder states.

In this work, we proceed to the relativistic two-valence coupled-cluster theory via the closed-shell [17] and one-valence coupled-cluster [18] theories reported in our previous works. We implement this within the framework of Fock-space or valence universal CCT [46,47]. The theory can be extended to systems with both particles and holes, however, for our present study an all-particle implementation is sufficient. Accordingly, the valence electrons are treated as particles [48] and each sector—closed-shell, one- and two-valence—are
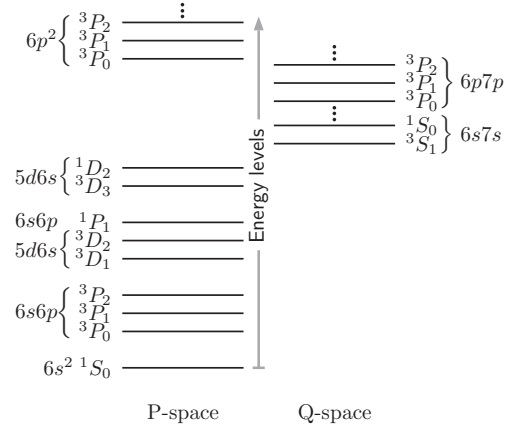

FIG. 3. Low-lying energy levels of atomic Yb.

separate Hilbert spaces. Technical advantage of Fock-space CCT with CMS is the sector-wise clean separation of cluster operators [49]. However, the Hilbert spaces of two-valence subsumes the one-valence after a direct product with a spectator valence state and similarly, the closed-shell after direct product with two-valence states. The state universal [50] is another flavor of open-shell CCT, where the wave operator is calculated in a single Hilbert space consisting of all the valence electrons. The wave operator is then state dependent and there is a lack of generality in the cluster equations. Furthermore, it requires complicated bookkeeping. These reasons have motivated us to choose the Fock-space CCT. Detailed discussions on Fock-space CCT and subtle issues related to the choice of model spaces are given in the review of Lindgren and Mukherjee [51].

A. Closed-shell and one-valence CCT

Coupled-cluster theory is a nonperturbative many-body theory. It is equivalent to selecting linked terms in the Bloch equation, Eq. (5), to all orders and combining terms of the same level of excitation (LOE). The elegance and perhaps all the attendant difficulties of CCT is the exponential nature of the wave operator. We provide a brief reprise of the closed-shell [17] and one-valence CCT [18]; these form the initial steps of the two-valence coupled-cluster theory. Indeed, a large fraction of the cluster amplitudes in the two-valence theory arise from the closed shell. The exact atomic wave function of a one-valence system in the coupled-cluster theory is

$$|\Psi_v\rangle = e^{(T+S)} = e^T(1+S)|\Phi_v\rangle, \tag{17}$$

where $|\Phi_v\rangle$ is the one-valence Dirac-Fock reference state, and T and S are the closed- and open-shell cluster operators, respectively. As evident from the equation, all the higher order terms (nonlinear) of T are calculated but S is restricted to linear terms only. The latter is on account of the single-valence electron. The diagrammatic representations of these operators are shown in Fig. 4. The closed-shell operator T in the coupled-cluster singles and doubles [21] approximation is
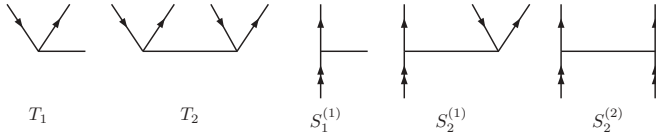
$$T = T_1 + T_2, \tag{18}$$

FIG. 4. Representation of the closed-shell and open-shell cluster operators.

where T_1 and T_2 are the single and double excitation operator, respectively. The closed-shell exact state in CCT is

$$|\Psi_0\rangle = e^T|\Phi_0\rangle, \tag{19}$$

and the cluster amplitudes are solutions of the nonlinear coupled equations,

$$\langle\Phi_a^p|\bar{H}_N|\Phi_0\rangle = 0, \tag{20}$$

$$\langle\Phi_{ab}^{pq}|\bar{H}_N|\Phi_0\rangle = 0, \tag{21}$$

where $\bar{H}_N = e^{-T}H_N e^T$ is the similarity transformed or dressed Hamiltonian. $|\Phi_0\rangle$, the Dirac-Fock reference state for the closed-shell part, is the eigenvalue of the central potential Hamiltonian H_0. And $|\Phi_a^p\rangle$ and $|\Phi_{ab}^{pq}\rangle$ are, respectively, the singly and doubly excited determinants. For details of the derivation, readers are referred to Ref. [17]. The open-shell cluster operator S is

$$S = S^{(1)} + S^{(2)}, \tag{22}$$

where $S^{(1)}$ and $S^{(2)}$ are the one-valence and two-valence cluster operators, respectively. Similar to T, the open-shell one-valence cluster operator $S^{(1)}$, in CCSD approximation, is of the form $S^{(1)} = S_1^{(1)} + S_2^{(1)}$. And these are solutions of the coupled linear equations,

$$\langle\Phi_v^p|\bar{H}_N + \overline{\{\bar{H}_N S^{(1)}\}}|\Phi_v\rangle = E_v^{\text{att}}\langle\Phi_v^p|S_1^{(1)}|\Phi_v\rangle, \tag{23}$$

$$\langle\Phi_{va}^{pq}|\bar{H}_N + \overline{\{\bar{H}_N S^{(1)}\}}|\Phi_v\rangle = E_v^{\text{att}}\langle\Phi_{va}^{pq}|S_2^{(1)}|\Phi_v\rangle. \tag{24}$$

In these equations E_v^{att} is the attachment energy of an electron to the v shell. It is defined as

$$E_v^{\text{att}} = E_v - E_0, \tag{25}$$

where $E_v = \langle\Phi_v|\bar{H}_N + \overline{\{\bar{H}_N S^{(1)}\}}|\Phi_v\rangle$ and $E_0 = \langle\Phi_0|\bar{H}|\Phi_0\rangle$ are the exact energy of $|\Psi_v\rangle$ and $|\Psi_0\rangle$, respectively. The excited determinants, $|\Phi_v^p\rangle$ and $|\Phi_{va}^{pq}\rangle$, are obtained by exciting an electron from valence orbitals to the virtuals. For detailed description of the derivation and interpretations, one may see Ref. [18].

Nonzero renormalization, right-hand side in Eqs. (23) and (24), is the predominant departure of open-shell CC from closed-shell CC. In the language of many-body diagrams, folded diagrams embody the renormalization terms. These, the folded diagrams, are topologically very different from the diagrams of $\bar{H}_N$ or $\overline{\bar{H}_N S^{(1)}}$. To illustrate the difference, folded diagrams from the two-valence CC are shown in Fig. 5. Strictly speaking, the distortion in these diagrams are introduced to obtain correct energy denominators with the diagrammatic evaluation in MBPT. CC being nonperturbative, there is no reason to be concerned about correct denominators. However, we retain the nomenclature
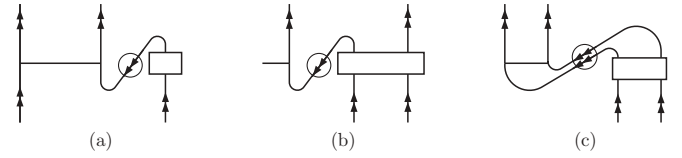

FIG. 5. Folded diagrams from the renormalization term in the generalized Bloch equation of two-valence systems. In two-valence coupled-cluster theory these diagrams arise from (a) $E_{vw}^{\text{att}}\langle\Phi_{vw}^{pq}|S_2^{(1)}|\Psi_{vw}\rangle$, (b)$E_{vw}^{\text{att}}\langle\Phi_{vw}^{pq}|S_1^{(1)}|\Psi_{vw}\rangle$, and (c)$E_{vw}^{\text{att}}\langle\Phi_{vw}^{pq}|S_2^{(2)}|\Psi_{vw}\rangle$.

and structure, in the diagrammatic analysis of CC equations, to identify the diagrams uniquely.

B. Two-valence CCT

In the two-valence sector, the cluster operator $S^{(2)} = S_2^{(2)}$ is a natural outcome of treating the single-valence excitations as a one-valence problem in Fock-space CCT. The exact two-valence state in CCT is

$$|\Psi_{vw}\rangle = e^T\left[1 + S_1^{(1)} + \tfrac{1}{2}S_1^{(1)2} + S_2^{(1)} + S_2^{(2)}\right]|\Phi_{vw}\rangle. \tag{26}$$

Here, for the valence part we have used $\exp(S) = 1 + S_1^{(1)} + (1/2)S_1^{(1)2} + S_2^{(1)} + S_2^{(2)}$. Notice that, although $(1/2)S_1^{(1)2}$ does not contribute to the one-valence CC equations, it does contribute to the two-valence CC equations. Using this in Eq. (2) and projecting on e^{-T}, we get

$$\bar{H}\left[1 + S_1^{(1)} + \tfrac{1}{2}S_1^{(1)2} + S_2^{(1)} + S_2^{(2)}\right]|\Phi_{vw}\rangle$$
$$= E_{vw}\left[1 + S_1^{(1)} + \tfrac{1}{2}S_1^{(1)2} + S_2^{(1)} + S_2^{(2)}\right]|\Phi_{vw}\rangle. \tag{27}$$

Hereafter for simplicity of representation we use $\exp(S) = 1 + S + (1/2)S^2$ with the definition, restricted to the two-valence sector only, $S^2 = S_1^{(1)2}$. Using the normal-ordered form the Hamiltonian, $H = H_N + E_{vw}^{\text{DF}}$, we can write

$$\bar{H}_N\left[1 + S + \tfrac{1}{2}S^2\right]|\Phi_{vw}\rangle = \Delta E_{vw}^{\text{corr}}\left[1 + S + \tfrac{1}{2}S^2\right]|\Phi_{vw}\rangle, \tag{28}$$

where $\Delta E_{vw}^{\text{corr}} = E_{vw} - E_{vw}^{\text{DF}}$ is the correlation energy of the two-valence atoms and, as defined earlier [Eq. (22)], $S = S^{(1)} + S^{(2)}$. Projecting the previous equation with $\langle\Phi_{vw}|$, we get the following expression for the correlation energy:

$$\langle\Phi_{vw}|\bar{H}_N\left[1 + S + \tfrac{1}{2}S^2\right]|\Phi_{vw}\rangle = \Delta E_{vw}^{\text{corr}}. \tag{29}$$

On the right-hand side we have used the relations $\langle\Phi_{vw}|S|\Phi_{vw}\rangle = 0$ and $\langle\Phi_{vw}|S^2|\Phi_{vw}\rangle = 0$, as the operation of S on the state $|\Phi_{vw}\rangle$ transforms it to an excited determinant orthogonal to $\langle\Phi_{vw}|$.

To obtain the two-valence cluster equations, we project Eq. (28) on the doubly excited determinants,

$$\langle\Phi_{vw}^{pq}|\bar{H}_N[1 + S + \tfrac{1}{2}S^2]|\Phi_{vw}\rangle = \Delta E_{vw}^{\text{corr}}\langle\Phi_{vw}^{pq}|S + \tfrac{1}{2}S^2|\Phi_{vw}\rangle, \tag{30}$$

where we have used $\langle \Phi_{vw}^{pq} | \Phi_{vw} \rangle = 0$. This equation can further be simplified, using Wick's theorem, as

$$\langle \Phi_{vw}^{pq} | \bar{H}_N + \{ \overparen{\bar{H}_N S} \} + \tfrac{1}{2} \{ \overparen{\bar{H}_N S^2} \} | \Phi_{vw} \rangle$$
$$= E_{vw}^{\text{att}} \langle \Phi_{vw}^{pq} | S + \tfrac{1}{2} S^2 | \Phi_{vw} \rangle, \qquad (31)$$

where E_{vw}^{att} is the difference between the exact energy of the closed-shell and two-valence states. It has the expression,

$$E_{vw}^{\text{att}} = \epsilon_v + \epsilon_w + \Delta E_{vw}^{\text{att}}, \qquad (32)$$

where ϵ_v and ϵ_w are the Dirac-Fock energy of the valence orbitals $|\phi_v\rangle$ and $|\phi_w\rangle$, respectively. And $\Delta E_{vw}^{\text{att}} = \Delta E_{vw}^{\text{corr}} - \Delta E_0^{\text{corr}}$ is the difference of the correlation energy of closed-shell and two-valence states. Diagrammatically, $\Delta E_{vw}^{\text{att}}$ in Eq. (32) is equivalent to the closed diagrams with free lines representing the valence states at the vertexes. Like in the second-order MBPT, one can separate the $\Delta E_{vw}^{\text{att}}$ diagrams to one- and two-body types. The one-body diagrams are similar to the ones in Fig. 1 with the bottom interaction (dotted line) replaced by cluster amplitude (solid line). Similarly, the two-body diagrams are similar to those of Figs. 2(b)–2(g) with the bottom interaction replaced by the cluster amplitude.

C. CC equation from Bloch equation

The CC equations discussed so far are derived from the eigenvalue equation of the Dirac-Coulomb Hamiltonian. Another approach is based on the generalized Bloch equation given in Eq. (5). This is more transparent to implement and convenient to analyze the working equations of CC with incomplete model space. In Eq. (5), the second term on the right-hand side, renormalization term, is often defined as

$$W = P V \Omega P = (V\Omega)_{\text{close}}. \qquad (33)$$

Here, *close* indicates the operator connects states within the model space. Diagrammatically, the representation of the operator has no free lines in the closed-shell sector and only valence orbitals as free lines in the open-shell sector. Using Eq. (33), we can write

$$[\Omega, H_0] P = (V\Omega - \Omega W) P. \qquad (34)$$

Operating on the two-valence atomic reference state, $|\Phi_{vw}\rangle$, and projecting with the doubly excited determinant $\langle \Phi_{vw}^{pq} |$, we get

$$\langle \Phi_{vw}^{pq} | [e^{T+S}, H_0] | \Phi_{vw} \rangle = \langle \Phi_{vw}^{pq} | [V e^T (1 + S + \tfrac{1}{2} S^2) - e^T (1 + S + \tfrac{1}{2} S^2) W] | \Phi_{vw} \rangle. \qquad (35)$$

From Wick's theorem further simplification follows after contracting the operators. There are connected and disconnected terms, however, only the connected terms remain [16] on both sides of Eq. (35). We get

$$\langle \Phi_{vw}^{pq} | \{ \overparen{H_0 S} \} - \{ \overparen{S H_0} \} | \Phi_{vw} \rangle$$
$$= -\langle \Phi_{vw}^{pq} | [V e^T (1 + S + \tfrac{1}{2} S^2) - e^T (1 + S + \tfrac{1}{2} S^2) W]_{\text{conn}} | \Phi_{vw} \rangle, \qquad (36)$$

where the subscript "conn" refers to connected terms. To arrive at the equation we have used $\langle \Phi_{vw}^{pq} | [T, H_0] | \Phi_{vw} \rangle = 0$, as T

being the closed-shell cluster operator, it does not operate in the valence space. To examine the equation in further detail, consider the terms on the right-hand side. Expanding the exponential in the term $V e^T$,

$$(V e^T)_{\text{conn}} = V + \{ \overparen{V T} \} + \frac{1}{2!} \{ \overparen{V T T} \} + \frac{1}{3!} \{ \overparen{V T T T} \}$$
$$+ \frac{1}{4!} \{ \overparen{V T T T T} \} = \bar{V}, \qquad (37)$$

where $\bar{V}$ is the dressed operator. Similarly, for the other terms,

$$(V e^T S)_{\text{conn}} = \{ \overparen{\bar{V} S} \}, \qquad (38)$$
$$(e^T S W)_{\text{conn}} = \{ \overparen{S W} \}, \qquad (39)$$
$$(e^T W)_{\text{conn}} = 0, \qquad (40)$$

as no contraction can occur between T, the closed-shell cluster operator, and open-shell operator S to obtain connected term. The same is true of T and the effective interaction W. The reason is, T operates on the closed-shell sector, whereas W operates in the valence sector. Though it is not shown explicitly, there are similar relations for $(1/2)S^2$ as well. From the definition of the normal Hamiltonian $\bar{H}_N = \bar{V} + \bar{H}_0$ we can combine two of the terms as

$$\overparen{\bar{H}_0 S} + \overparen{\bar{V} S} = \overparen{\bar{H}_N S}. \qquad (41)$$

Using Eqs. (37)–(40) in Eq. (36) we get the CC equation in the form,

$$\langle \Phi_{vw}^{pq} | \bar{H}_N + \{ \overparen{\bar{H}_N S} \} + \tfrac{1}{2} \{ \overparen{\bar{H}_N SS} \} - \overparen{S H_{\text{eff}}}$$
$$- \tfrac{1}{2} \{ \overparen{S H_{\text{eff}}} \} | \Phi_{vw} \rangle = 0, \qquad (42)$$

where $H_{\text{eff}} = H_0 + W$ is the effective Hamiltonian. The form of the effective Hamiltonian H_{eff} is close—no free lines or only valence lines as free lines—therefore Eq. (42) can be written as

$$\langle \Phi_{vw}^{pq} | \bar{H}_N + \{ \overparen{\bar{H}_N S} \} + \tfrac{1}{2} \{ \overparen{\bar{H}_N S^2} \} | \Phi_{vw} \rangle$$
$$= H_{\text{eff}} \langle \Phi_{vw}^{pq} | S + \tfrac{1}{2} S^2 | \Phi_{vw} \rangle. \qquad (43)$$

This is identical to Eq. (31), which is obtained from the eigenvalue equation of the Dirac-Coulomb Hamiltonian with the exponential ansatz.

D. Diagonalization of H_{eff}

In the single reference calculations the mapping from reference state to exact state is simple and straightforward. The exact state, as given in Eq. (4), is the transformation of reference state $|\Phi_{vw}\rangle$ with Ω. It is not so simple with multireference model spaces. The model space then encompasses a set of determinantal states $\{|\Phi_{v_\alpha w_\beta}\rangle\} \in P$, however, each state by

itself is not the reference state. The CC equation in Eq. (43) is then modified to

$$\langle \Phi^{pq}_{v_\alpha w_\beta} | \bar{H}_N + \overbrace{\{\bar{H}_N S\}} + \frac{1}{2} \overbrace{\{\bar{H}_N S S\}} | \Phi_{v_\alpha w_\beta} \rangle$$
$$- \sum_{\gamma,\delta} \langle \Phi^{pq}_{v_\alpha w_\beta} | \overbrace{S + \frac{1}{2} S^2 | \Phi_{v_\gamma w_\delta} \rangle \langle \Phi_{v_\gamma w_\delta} | W} | \Phi_{v_\alpha w_\beta} \rangle = 0,$$

(44)

where, the sum over δ and γ spans all the determinantal states within P. This is the working equation of multireference two-valence CCT with CMS. The last term requires careful consideration while implementing and as we mentioned earlier, folded diagrams arise from this term.

The wave operator Ω is defined once the CC equations are solved, but the model functions are not yet defined. Next step of the calculation is then to evaluate the matrix elements of the effective Hamiltonian,

$$H_{\text{eff}}(v,w;x,y) = \langle \Phi_{vw} | H_0 + V\Omega | \Phi_{xy} \rangle. \tag{45}$$

The H_{eff} matrix is nonsymmetric as Ω operates on the ket state and after diagonalization, one gets a biorthogonal set of eigenstates $|\Psi^0_i\rangle$. These are the model functions of the multireference CC, the exact state is then

$$|\Psi_i\rangle = \Omega |\Psi^0_i\rangle, \tag{46}$$

and the eigenvalue equation is

$$H_{\text{eff}} |\Psi^0_i\rangle = E_i |\Psi^0_i\rangle. \tag{47}$$

The eigenstates in general are of the form,

$$|\Psi^0_i\rangle = \sum_{\alpha\beta} c^i_{\alpha\beta} |\Phi_{v_\alpha w_\beta}\rangle, \tag{48}$$

where $c^i_{\alpha\beta}$ are the coefficients of the linear combination or eigenvector elements of H_{eff}.

IV. INCOMPLETE MODEL SPACE

Incomplete model space (IMS) consists of a restricted number of configurations from the CMS. Remaining configurations are part of the orthogonal space. The outcome of such a model space is that the clean separation of internal and external cluster amplitudes is no longer true. Furthermore, the subsystem embedding condition is violated. For example, cluster operators which are external in one-valence Hilbert space may no longer be so in the two-valence Hilbert space. The intermediate normalization Eq. (6) is then, in general, not applicable:

$$|\Psi^0_i\rangle \neq P\Omega |\Psi^0_i\rangle. \tag{49}$$

Following that the H_{eff} is not guaranteed to be operational only within the model space, it may as well connect a state in P to a state in Q, whereas the obvious advantage of defining H_{eff} is to work within the model space and incorporate the effects of orthogonal space in an effective way. Restoring the operational space of H_{eff} to P requires a set of constraint equations [49], and a previous work reported the implementation of particle-hole sectors [52] in relativistic CC calculations. However, all the good virtues of CMS, in the context of Fock-space CCT,
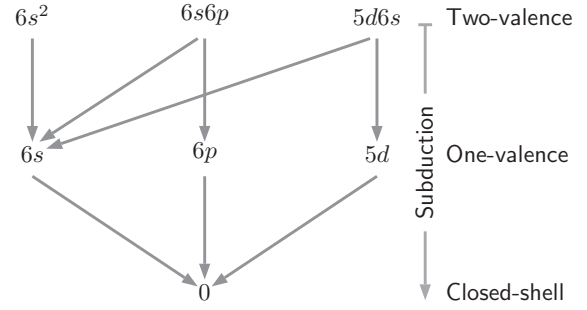

FIG. 6. Incomplete model space of Yb two-valence calculations. Arrows indicate the *subduction* to lower valence sectors and respective model spaces.

are applicable when the model space is quasicomplete. For a lucid description of what constitutes a quasicomplete model space refer to Refs. [43,51].

Like in CMS, as a specific example consider the low-lying states of Yb. An ideal incomplete model space would consist of the configurations $6s^2$, $6s6p$, and $5d6s$. Model space would then encompass all the levels important to ongoing precision experiments: $6s^2(^1S_0)$, $6s6p(^3P_J)$, $5d6s(^3D_J)$, and $6s6p(^1P_1)$. An obvious advantage in such a selection of model space is isolation, as evident in Fig. 3, from the potential *intruder* states $6p7p(^3P_J)$, $6s7s(^3S_1)$, and $6s7s(^1S_0)$. Here, we can apply the subduction process to check if the model space considered is quasicomplete (shown in Fig. 6).

The initial stage is the two-valence model space consisting of $6s^2$, $6s6p$, and $5d6s$. Removal of one electron from each of the configurations leads to a configuration in one-valence model space ($6s$, $6p$, and $5d$). Finally, removal of another electron gives the closed-shell model space. All the configurations obtained in the subduction are part of respective model spaces. This is a requirement of quasicomplete model space and necessary condition for separation of internal and external excitations.

V. PROPERTIES CALCULATIONS

A. Hyperfine structure constants

The HFS constants of an atom are the parameters which measure further splitting of fine structure levels. It arises from the interaction of electromagnetic moments of the nucleus with the electromagnetic field of the atomic electrons [53]. The general form of the hyperfine interaction Hamiltonian is

$$H_{\text{hfs}} = \sum_i \sum_{k,q} (-1)^q t^k_q(\hat{\mathbf{r}}_i) T^k_{-q}, \tag{50}$$

where $t^k_q(\mathbf{r})$ and T^k_q are irreducible tensor operators of rank k effective in the electron and nuclear spaces, respectively. For the magnetic dipole interaction ($k = 1$), the explicit form of the tensor operators are

$$t^1_q(\mathbf{r}) = \frac{-i\sqrt{2}[\boldsymbol{\alpha} \cdot \mathbf{C}_1(\hat{\mathbf{r}})]_q}{cr^2},$$
$$T^1_q = \mu_q. \tag{51}$$

Here, $\mathbf{C}_1(\hat{\mathbf{r}})$ is a rank one tensor operator in electron space and μ_q is a component of $\boldsymbol{\mu}$, the nuclear magnetic moment

operator. The HFS constants are the expectation value of H_{hfs} and the magnetic dipole HFS constant is then

$$a = \frac{\langle \Psi_i | H_{\mathrm{hfs}} | \Psi_i \rangle}{\langle \Psi_i | \Psi_i \rangle}, \qquad (52)$$

where $|\Psi^i\rangle$ is the exact wave function expressed in Eq. (17), using coupled-cluster theory. The denominator $\langle \Psi_i | \Psi_i \rangle$ is the normalization factor and it is not to be confused with intermediate normalization Eq. (6). The later defines the relation between the reference state and the exact state. And it does not determine the normalization of the exact state.

B. HFS constant in one-valence sector

Once the CC equations and cluster amplitudes are known, the atomic properties are calculated with the exact atomic states so obtained. It is the expectation for dynamical variables and the matrix element for transition amplitudes. From the CC wave function of one-valence systems in Eq. (17), the expectation of H_{hfs} is

$$\langle \Psi_v | H_{\mathrm{hfs}} | \Psi_v \rangle = \langle \Phi_v | \tilde{H}_{\mathrm{hfs}} + 2S^\dagger \tilde{H}_{\mathrm{hfs}} + S^\dagger \tilde{H}_{\mathrm{hfs}} S | \Phi_v \rangle, \quad (53)$$

where $\tilde{H}_{\mathrm{hfs}} = e^{T^\dagger} H_{\mathrm{hfs}} e^T$ is the dressed operator. The factor of two in the second term on the right-hand side accounts for $\tilde{H}_{\mathrm{hfs}} S$ as $S^\dagger \tilde{H}_{\mathrm{hfs}} = \tilde{H}_{\mathrm{hfs}} S$. An expansion of $\tilde{H}_{\mathrm{hfs}}$ ideal for an order-wise calculation is

$$\tilde{H}_{\mathrm{hfs}} = H_{\mathrm{hfs}} e^T + \sum_{n=1}^{\infty} \frac{1}{n!} (T^\dagger)^n H_{\mathrm{hfs}} e^T. \qquad (54)$$

The normalization factor, denominator in Eq. (52), in terms of the coupled-cluster wave function is

$$\langle \Psi_v | \Psi_v \rangle = \langle \Phi_v | (1 + S^\dagger) e^{T^\dagger} e^T (1 + S) | \Phi_v \rangle. \qquad (55)$$

Note that the dressed operator $\tilde{H}_{\mathrm{hfs}}$ and $e^{T^\dagger} e^T$ in the normalization factor are nonterminating series. In a recent work, we demonstrated a scheme to include a class of diagrams to all order in T iteratively for properties calculations. With the method we calculated the magnetic dipole HFS constant of the singly ionized alkaline-earth metals [18]. Based on the extensive calculations reported in Ref. [18], we conclude terms higher than quadratic in T contribute less than 0.1% to the HFS constants. So there are no compromises on important physics when $\tilde{H}_{\mathrm{hfs}}$, Eq. (57), is truncated after the second order in T. However, there are enormous gains in computing resources and simplification of the procedure with the iterative scheme. Here, we shall not dwell on the iterative scheme; interested readers may refer to Ref. [18] for more details.

C. HFS constant in two-valence systems

From the CC wave functions of two-valence systems defined in Eq. (26), we get

$$\langle \Psi_i | H_{\mathrm{hfs}} | \Psi_i \rangle = \sum_{j,k} c_j^{i*} c_k^i \left[\langle \Phi_j | \tilde{H}_{\mathrm{hfs}} + \tilde{H}_{\mathrm{hfs}} \left(S + \frac{1}{2} S^2 \right) \right.$$
$$+ \left(S + \frac{1}{2} S^2 \right)^\dagger \tilde{H}_{\mathrm{hfs}} + \left(S + \frac{1}{2} S^2 \right)^\dagger$$
$$\times \left. \tilde{H}_{\mathrm{hfs}} \left(S + \frac{1}{2} S^2 \right) | \Phi_k \rangle \right], \qquad (56)$$
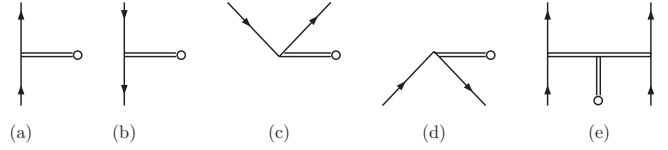

(a) (b) (c) (d) (e)

FIG. 7. Representation of effective one- and two-body dressed properties operators.

where to shorten the notations we have replaced the valence indexes in the two-valence states $v_\alpha w_\beta$ ($v_\delta w_\gamma$) with j (k). This is the CC expression to calculate the HFS constants of two-valence electron atoms. The operator $\tilde{H}_{\mathrm{hfs}}$ is, as defined earlier, the dressed HFS interaction Hamiltonian. As discussed in the one-valence case, comprehensive inclusion of all order of T is beyond the scope of current theories and computational resources. Hence, for the two-valence sector we consider up to quadratic terms of T in $\tilde{H}_{\mathrm{hfs}}$, approximately

$$\tilde{H}_{\mathrm{hfs}} \approx H_{\mathrm{hfs}} + H_{\mathrm{hfs}} T + T^\dagger H_{\mathrm{hfs}} + T^\dagger H_{\mathrm{hfs}} T. \qquad (57)$$

To compute $\tilde{H}_{\mathrm{hfs}}$ of the two-valence sector, we borrow the concept of effective one- and two-body operators from our previous work in Ref. [18]. Diagrammatic representation of the effective operators are as shown in Fig. 7. It is important to note that the two-body effective operator, shown in Fig. 7(e), arises from the last term in Eq. (57). And, since it has two orders of T, the actual hyperfine diagrams obtained after contraction with S may have negligible contributions. For this reason we shall not elaborate on the HFS diagrams arising from the dressed two-body effective properties operator. However, we do incorporate these diagrams in the calculations and mention the contributions in the results.

The diagrams of the HFS constant in the two-valence sector are grouped into different categories—first based on the cluster operators in the expression and later, in terms of the number of core, valence, and virtual orbitals. Specific terms and groups of diagrams are discussed in this work.

1. Effective one-body operator

There are four diagrams from $\tilde{H}_{\mathrm{hfs}}$ which has nonzero contribution. These are the two-valence diagrams from $T_2^\dagger T_2$ with the bare hyperfine interaction h_{hfs} inserted to all the possible orbital lines. Contributions from these diagrams is expected to be very small as S are not a part of the diagrams.

Diagrammatically, $\tilde{H}_{\mathrm{hfs}} S^{(1)}$ and $S^{(1)\dagger} \tilde{H}_{\mathrm{hfs}}$ each have one diagram and these arise when $S^{(1)}$ is contracted with the one-body effective operators: $S_2^{(1)}$ with diagram in Fig. 7(d), and $S_2^{(1)\dagger}$ with diagram in Fig. 7(c). The diagram arising from $S_2^{(1)\dagger} \tilde{H}_{\mathrm{hfs}}$ is as shown in Fig. 8(a). The time-reversed version of the same diagram corresponds to $\tilde{H}_{\mathrm{hfs}} S_2^{(1)}$, however, this is not shown in the figure. The contributions from $\tilde{H}_{\mathrm{hfs}} S^{(1)}$ and $S^{(1)\dagger} \tilde{H}_{\mathrm{hfs}}$ are large as these are only first order in S. Furthermore, H_{hfs} is a one-body interaction and hence, one-body effective interactions are dominant.

The terms $\tilde{H}_{\mathrm{hfs}} S^{(2)}$ and $S^{(2)\dagger} \tilde{H}_{\mathrm{hfs}}$ each have one diagram and these arise from the contraction of $S_2^{(2)}$ with the one-body effective operator of $\tilde{H}_{\mathrm{hfs}}$ shown in diagram Fig. 7(a).
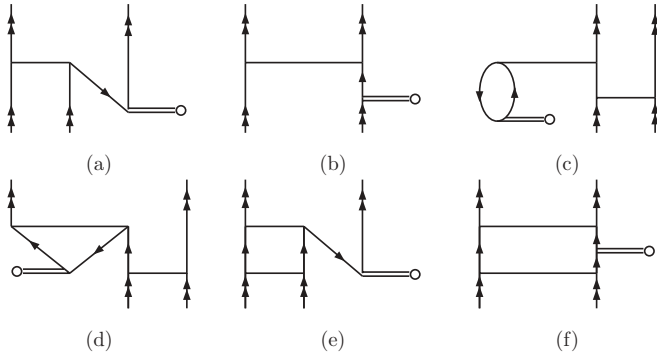
FIG. 8. Hyperfine diagrams contributing to the terms, $S_2^{(1)\dagger}\widetilde{H}_{\text{hfs}}$ (a), $S^{(2)\dagger}\widetilde{H}_{\text{hfs}}$ (b), $S_2^{(1)\dagger}\widetilde{H}_{\text{hfs}}S^{(2)}$ [(c)–(e)], and $S^{(2)\dagger}\widetilde{H}_{\text{hfs}}S^{(2)}$ (f).

The diagram from $S^{(2)\dagger}\widetilde{H}_{\text{hfs}}$ is shown in Fig. 8(b). Like in the previous case, the time-reversed diagram arises from $\widetilde{H}_{\text{hfs}}S^{(2)}$ and is not shown in the figure. One can expect these terms to constitute the leading order as these are the lowest order terms with $S_2^{(2)}$. Rationale for such an anticipation is, in general, that the magnitudes of $S_2^{(2)}$ are larger than the $S_2^{(1)}$ and T operators.

2. $S^\dagger \widetilde{H}_{\text{hfs}} S$

The leading term in Eq. (56) which is quadratic in S is

$$S^\dagger \tilde{H}_{\text{hfs}} S = S^{(1)\dagger} \tilde{H}_{\text{hfs}} S^{(1)} + [S^{(2)\dagger} \tilde{H}_{\text{hfs}} S^{(1)} + \text{c.c.}] + S^{(2)\dagger} \tilde{H}_{\text{hfs}} S^{(2)}, \quad (58)$$

where c.c. represents complex conjugation. We now discuss the diagrams arising from each of these terms. There are 16 diagrams arising from $S^{(1)\dagger}\widetilde{H}_{\text{hfs}}S^{(1)}$ and topologically, these are the effective one-body diagrams Figs. 7(a) and 7(b) sandwiched between $S^{(1)\dagger}$ and $S^{(1)}$. To examine the diagrams in more detail, all the diagrams (four in all) from the contraction $\overline{S_2^{(1)\dagger} S_2^{(1)}}$ are shown in Fig. 9. To each of the diagrams in Fig. 9 the effective one-body operator can be inserted in four ways. As an example, consider the diagram in Fig. 9(b); all the four diagrams after inserting the effective one-body operator are shown in Fig. 10.

There are five diagrams from $S^{(1)\dagger}\widetilde{H}_{\text{hfs}}S^{(2)}$. These arise from the contraction of $S^{(1)\dagger}$ with $S^{(2)}$ through one-body operators in Figs. 7(a) and 7(c). The diagrams from $S_2^{(1)\dagger}\widetilde{H}_{\text{hfs}}S^{(2)}$ are as shown in Figs. 8(c)–8(e). However, the diagrams from $S_1^{(1)\dagger}$ are not shown. An identical number of diagrams arise from $S^{(2)\dagger}\widetilde{H}_{\text{hfs}}S^{(1)}$. The effective diagram in this case are Figs. 7(a) and 7(d).

Finally, only one diagram arises from the last term, $S^{(2)\dagger}\widetilde{H}_{\text{hfs}}S^{(2)}$. This diagram is shown in Fig. 8(f). Only Fig. 7(a)
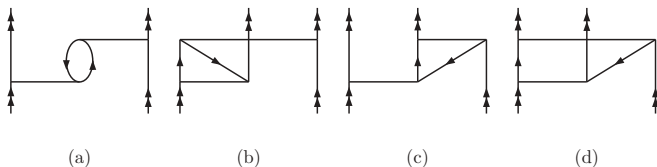

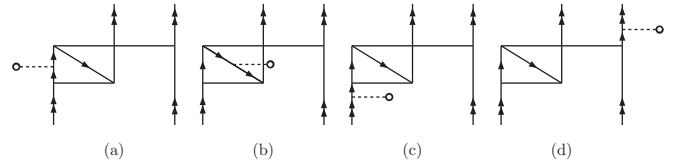FIG. 9. Diagrams arising from contraction of $S_2^{(1)\dagger}$ with $S_2^{(1)}$.

FIG. 10. Hyperfine diagrams obtained after inserting the hyperfine interaction operator in diagram (b) of Fig. 9.

is the allowed effective one-body operator which contributes to this term.

D. Electric dipole transition amplitudes

Electric dipole is the most dominant electromagnetic multipole in the radiative transition of atoms. In a majority of the cases, depending on the decay channels, it defines the lifetime of an excited state. Theoretically, the relevant quantity is the reduced matrix element of the dipole operator **D** between the initial and final states $|\Psi_i\rangle$ and $|\Psi_f\rangle$, respectively. The two states are opposite in parity as **D** is an odd parity operator. The expression of the reduced matrix element is

$$D_{if} = \frac{\langle\Psi_f||D||\Psi_i\rangle}{\sqrt{\langle\Psi_f|\Psi_f\rangle\langle\Psi_i|\Psi_i\rangle}}. \quad (59)$$

Once the reduced matrix elements are evaluated, the actual matrix elements of the specific states are calculated from the Wigner-Eckert theorem. Here, we need to make a finer distinction of the wave operator in the valence universal or Fock-space CCT. As H^{DC} commutes with parity, so does the wave operator Ω and we can consider Ω as

$$\Omega = \Omega^+ + \Omega^-, \quad (60)$$

where Ω^+ and Ω^- operates on the even and odd parity reference states within the model space. The separation of these two components follows naturally from the parity selection rules imposed on the cluster amplitudes. However, this ought to be handled with care as complications arise in the calculations of perturbed cluster amplitudes where there is a second perturbation, besides the residual Coulomb interaction, which is parity odd. We may rewrite Eq. (59) more precisely as

$$D_{if} = \frac{\langle\Psi_f^0||\Omega^{\mp\dagger}D\Omega^\pm||\Psi_i^0\rangle}{\sqrt{\langle\Psi_f|\Psi_f\rangle\langle\Psi_i|\Psi_i\rangle}}. \quad (61)$$

In the one-valence sector, the reduced matrix element of D is

$$\langle\Psi_w||D||\Psi_v\rangle = \langle\Phi_v||\tilde{D} + S^\dagger\tilde{D} + \tilde{D}S + S^\dagger\tilde{D}S||\Phi_v\rangle, \quad (62)$$

where $|\Psi_v\rangle$ and $|\Psi_w\rangle$ are the initial and final states in terms of the valence states. Though the expressions are similar to Eq. (53), there are two important differences. Unlike the HFS energy splitting expression $S^\dagger\tilde{D} \neq \tilde{D}S$, this is because the initial and final states are different. The same set of properties diagrams in HFS calculations, after modifications to account for the two key differences, is then adopted to compute reduced **D** matrix elements with CC wave functions.

After a similar modification, like in Eq. (56), for the two-valence systems,

$$
\langle \Psi_f || D || \Psi_i \rangle = \sum_{j,k} c_j^{f^*} c_k^i \left[\langle \Phi_j | \tilde{D} + \tilde{D} \left(S + \frac{1}{2} S^2 \right) \right.
$$

$$
+ \left(S + \frac{1}{2} S^2 \right)^\dagger \tilde{D} + \left(S + \frac{1}{2} S^2 \right)^\dagger,
$$

$$
\left. \times \ \tilde{D} \left(S + \frac{1}{2} S^2 \right) | \Phi_k \rangle \right], \tag{63}
$$

where the notations and terms are the same as in the two-valence HFS case. However, the two key differences mentioned earlier still hold true. Like in HFS,

$$
\tilde{D} \approx D + DT + T^\dagger D + T^\dagger DT. \tag{64}
$$

We then proceed like in HFS and calculate the effective diagrams, both one and two body. These are then contracted with the cluster operators and we evaluate the transition matrix.

VI. NUMERICAL DETAILS

Coupled-cluster theory, though powerful, is computationally intensive and implementation is nontrivial. The large number of unknowns and equations demand special attention to all aspects of computations—right from the initial stage of identifying and calculating the cluster diagrams, to the final stages of solving the CC equations and computing properties from the CC wave functions. Here, we give a concise description of what we consider absolutely essential, theoretical, and computational aspects for atomic coupled-cluster calculations. This choice is entirely based on our experience of developing and implementing CCT spanning closed-shell, one-, and two-valence systems. Besides the CC wave-function calculations, we have also proposed, developed, and implemented methods to compute properties from CC wave functions. The selected issues addressed are provided with the anticipation that interested researchers shall find these details valuable and facilitate adopting CCT for atomic many-body computations with minimal effort.

A. Orbitals and basis functions

Results presented in this paper are based on the Dirac-Coulomb Hamiltonian H^{DC} given in Eq. (1). It incorporates relativity at the single-particle level accurately and, as the name indicates, the Coulomb interactions between the electrons. For the nuclear potential $V_N(r)$, we consider the finite size Fermi density distribution,

$$
\rho_{\mathrm{nuc}}(r) = \frac{\rho_0}{1 + e^{(r-c)/a}}, \tag{65}
$$

here, $a = t4 \ln 3$. The parameter c is the half-charge radius, that is, $\rho_{\mathrm{nuc}}(c) = \rho_0/2$ and t is the skin thickness. At the single-particle level, the spin orbitals are of the form,

$$
\psi_{n\kappa m}(\mathbf{r}) = \frac{1}{r} \begin{pmatrix} P_{n\kappa}(r) \chi_{\kappa m}(\mathbf{r}/r) \\ i \, Q_{n\kappa}(r) \chi_{-\kappa m}(\mathbf{r}/r) \end{pmatrix}, \tag{66}
$$

where $P_{n\kappa}(r)$ and $Q_{n\kappa}(r)$ are the large and small component radial wave functions, κ is the relativistic total angular momentum quantum number, and $\chi_{\kappa m}(\mathbf{r}/r)$ are the spin or spherical

harmonics. One representation of the radial components is to define these as a linear combination of Gaussian-like functions and are referred to as Gaussian-type orbitals (GTOs). Then, the large and small components [54,55] are

$$
P_{n\kappa}(r) = \sum_p C_{\kappa p}^L g_{\kappa p}^L(r),
$$

$$
Q_{n\kappa}(r) = \sum_p C_{\kappa p}^S g_{\kappa p}^S(r). \tag{67}
$$

The index p varies over the number of the basis functions. For the large component we choose

$$
g_{\kappa p}^L(r) = C_{\kappa i}^L r^{n_\kappa} e^{-\alpha_p r^2}, \tag{68}
$$

where n_κ is an integer. Similarly, the small component is derived from the large components using kinetic balance condition [56]. The exponents in the previous expression follow the general relation,

$$
\alpha_p = \alpha_0 \beta^{p-1}. \tag{69}
$$

The parameters α_0 and β are optimized for each of the ions or neutral atoms to provide a good description of the properties. In our case the optimization criteria are to reproduce the numerical result of the self-consistent field (SCF) energy and orbital energies.

From Eq. (66) the reduced matrix element of the magnetic hyperfine operator between two spin orbitals, v' and v, is

$$
\langle v' || t^1 || v \rangle = -(\kappa_v + \kappa_{v'}) \langle -\kappa_{v'} || C^1 || \kappa_v \rangle
$$

$$
\times \int_0^\infty \frac{dr}{r^2} (P_{n_{v'}\kappa_{v'}} Q_{n_v \kappa_v} + Q_{n_{v'}\kappa_{v'}} P_{n_v \kappa_v}). \tag{70}
$$

A detailed derivation is given in Ref. [57].

For the alkaline-earth-metal atoms Sr and Ba as well as Yb, we use V^{N-2} orbitals for the calculations. This is equivalent to calculating the spin orbitals from the single-particle eigenvalue equations of the doubly ionized atoms, namely Sr^{2+}, Ba^{2+}, and Yb^{2+}. The single-particle basis sets then have few bound states and the rest are continuum. The basis set is optimized such that single-particle energies of the core and valence orbitals are in good agreement with the numerical results. For this we use GRASP92 [58] to generate the numerical results.

B. Orbital subsets

Orbitals, the single electron wave functions, in closed-shell systems are separated into two distinct subsets: core (occupied) and virtual (unoccupied). The former are shells which are completely filled in the ground-state determinantal state and later are empty. Distinction is not so straightforward in open-shell systems. The classification of the orbitals for the Yb atom in our current calculations is shown in Fig. 11. The valence orbitals are partially filled in the model functions and are like core orbitals; electrons can be excited from the valence shells.

This is particularly true when considering the valence as particles. Consequently, as discussed in the next subsection, the closed-shell diagrams can be modified to the open-shell ones. On the other hand, valence shells can also accommodate excitations from the core shells, a property typical of shells in the virtual space. Hence, in the cluster amplitudes the excited states incorporate the valence orbitals as well. The dual character of the valence orbitals can be adapted for
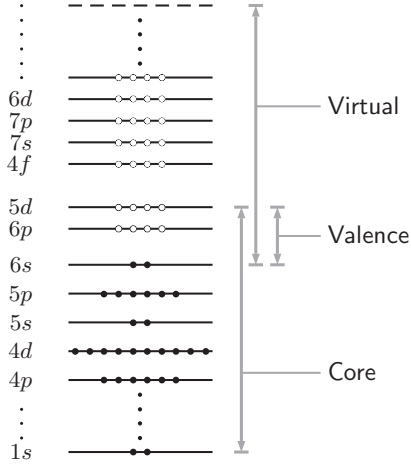
FIG. 11. Classification of orbitals into core, valence, and virtual subsets. Few orbitals are members of more than one subset.

FIG. 12. Conversion from closed-shell cluster operator T diagrams to open-shell operators S, (a) closed-shell cluster diagram, (b) one-valence cluster diagram, and (c) two-valence cluster diagram.

faster diagram evaluations with appropriate rearrangement of the summation sequence. For example, there is enormous computational advantage in considering the free orbital lines, in the cluster diagrams, as the outermost summation. The example given and many other features we have developed are more computational in nature and less of physics. We shall elaborate on these matters in future publications devoted to the computational aspects of our work.

C. CC equations

In Fock-space CCT, as mentioned earlier, the cluster operators are generated sector-wise in sequence. First, the closed-shell cluster amplitudes are computed from Eqs. (20) and (21), where the dressed operator $\bar{H}_N$ in the closed-shell CC equations, like in Eq. (37), is

$$\bar{H}_N = H_N + \{H_N \overset{\sqcap}{T}\} + \frac{1}{2!}\{H_N \overset{\sqcap}{TT}\} + \frac{1}{3!}\{H_N \overset{\sqcap}{TTT}\}$$
$$+ \frac{1}{4!}\{H_N \overset{\sqcap}{TTTT}\}. \tag{71}$$

The closed-shell CC equations as evident from the expression of $\bar{H}_N$ are nonlinear equations. In CCSD approximation, we have second- and fourth-order nonlinearities in T_2 and T_1, respectively. However, the working equations can be written in linear form as

$$A_{11}(T)T_1 + A_{12}(T)T_2 = B_1, \tag{72}$$
$$A_{21}(T)T_1 + A_{22}(T)T_2 = B_2. \tag{73}$$

Since the original equations are nonlinear equations, the coefficients $A_{ij}(T)$ are functions of cluster amplitudes T. On the right side B are the matrix elements of H_N. The equations are then solved iteratively until convergence.

To set up the equations, we evaluate the terms based on diagrammatic analysis. There are several diagrams and, for example, those arising from linear terms are given in Ref. [16]. The total number of equations scale as $N_v^2 N_o^2$, where N_v and N_o are number of virtual and occupied orbitals, respectively. For the calculations discussed in this paper $N_v \approx 130$ or more and $N_o \approx 20$. The coefficient matrix A is nonsymmetric and dense, so the number of matrix elements scales as $\sim N_v^4 N_o^4$, which is
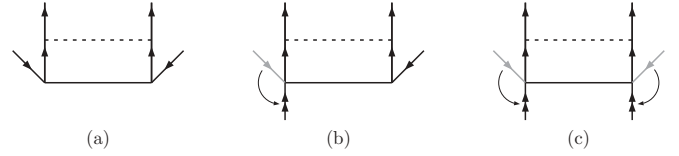
$\sim 4.6 \times 10^{13}$ for typical examples in the present computations. It is an extremely large matrix and impractical to store. In addition, the elements are functions of T and not static. For these reasons, the elements of A are calculated on the fly, as and when needed. Another complication is the operations required to generate each element of A in the equations scale as $N_v^4 N_o^2$, all together, combining the number of matrix elements and number of operations, number of binary arithmetic operation in each iteration is $O(N_v^8 N_o^6)$, which is indeed a very large number for high-Z atoms.

Diagrammatically, to generate the closed-shell equations, we identify all the diagrams in the closed-shell CC equations and evaluate the angular integrations based on angular momentum diagrams [16]. An example diagram is shown in Fig. 12(a), and it is the double contraction of V with T_2 and contributes to the T_2 equation. To set up the one-valence and two-valence cluster equations we avoid diagrammatic evaluation. Instead, the closed-shell diagrams are topologically transformed into one-valence diagrams. As shown in Fig. 12(b), one of the core orbital lines is rotated and transformed into a valence line. Diagrams so obtained are very different from Fig. 12(a) in terms of possible contractions. However, the results from the angular integration remain unchanged. A similar procedure is adopted for the two-valence equations as well. With this, a careful analysis and evaluation of closed-shell CC equations is the only requirement to set up the one- and two-valence CC equations. The coupled nonlinear and linear equations are solved iteratively. We employ direct inversion in the iterated subspace (DIIS) [59] for convergence acceleration.

VII. RESULTS

A. Excitation energies

Excitation energies of the one-valence ions Sr$^+$ and Ba$^+$ were reported in our previous paper [18]. Here, we report the results of the calculations in the two-valence sector, the excitation energy of a state $nln'l'\,^{(2S+1)}L_J$, from Eq. (47), is

$$\Delta E_{nln'l'\,^{(2S+1)}L_J} = E_{nln'l'\,^{(2S+1)}L_J} - E_{ns^2\,^1S_0}, \tag{74}$$

where $E_{ns^2\,^1S_0}$ and $E_{nln'l'\,^{(2S+1)}L_J}$ are the ground and excited state eigenvalues of H_{eff} in Eq. (47). Vaeck, Godfroid, and Hansen [60] had calculated the excitation energies and investigated in detail the configuration mixing of atomic Sr with multiconfiguration Hartree-Fock theory with special attention on the singlet states ^1L. In particular, the states with configurations of the form $5snp\,^1P^\circ$, $5snd\,^1D$, and $5snf\,^1F^\circ$, including the Rydeberg states. Improved experimental data and prospects of cooling and trapping had spurred further theoretical studies on properties of Sr. Important recent theoretical work are by Porsev and collaborators [61], and Savukov and Johnson

TABLE I. Two-electron removal energy and the excitation energies calculated using relativistic coupled-cluster theory. All values are in atomic units.

State	Our result		Other work	Expt. result Ref. [63].
	E_{vw}	EE	EE	EE
Atomic ^{87}Sr; [Kr]$5s^2$				
$5s^2\ ^1S_0$	−0.61939	0.0	0.0	0.0
$5s5p\ ^3P_0$	−0.55169	0.06771	0.06566[a]	0.06524
$5s5p\ ^3P_1$	−0.55170	0.06768	0.06651,[a] 0.06871[b]	0.06609
$5s5p\ ^3P_2$	−0.55203	0.06736	0.06833[a]	0.06788
$5s4d\ ^3D_1$	−0.53551	0.08388	0.08230[a]	0.08274
$5s4d\ ^3D_2$	−0.53478	0.08461	0.08260[a]	0.08301
$5s4d\ ^3D_3$	−0.53397	0.08542	0.08312[a]	0.08347
$5s4d\ ^1D_2$	−0.52594	0.09345	0.09210,[a] 0.11477[c]	0.09181
$5s4d\ ^1P_1$	−0.51283	0.10656	0.09851,[a] 0.10015,[b] 0.10730[c]	0.09887
Atomic ^{137}Ba; [Xe]$6s^2$				
$6s^2\ ^1S_0$	−0.56439	0.0	0.0	0.0
$6s5d\ ^3D_1$	−0.52303	0.04136	0.04211,[d] 0.04106,[e] 0.04119[f]	0.04116
$6s5d\ ^3D_2$	−0.52170	0.04269	0.04296,[d] 0.04193,[e] 0.04200[f]	0.04199
$6s5d\ ^3D_3$	−0.51960	0.04479	0.04473,[d] 0.04375,[e] 0.04366[f]	0.04375
$6s5d\ ^1D_2$	−0.51030	0.05409	0.05395,[d] 0.05197,[e] 0.05298[f]	0.05192
$6s6p\ ^3P_0$	−0.50667	0.05772	0.05697,[d] 0.05575,[e] 0.05591[f]	0.05589
$6s6p\ ^3P_1$	−0.50540	0.05899	0.05869,[d] 0.05742,[e] 0.05758[f]	0.05758
$6s6p\ ^3P_2$	−0.50311	0.06128	0.06284,[d] 0.06147,[e] 0.06159[f]	0.06158
$6s6p\ ^1P_1$	−0.47291	0.09148	0.08409,[d] 0.08256,[e] 0.08125[f]	0.08229
Atomic ^{173}Yb; [Xe]$4f^{14}6s^2$				
$6s^2\ ^1S_0$	−0.68083	0.0	0.0	0.0
$6s6p\ ^3P_0$	−0.59944	0.08140	0.07909,[g] 0.07874,[h] 0.07877[i]	0.07877
$6s6p\ ^3P_1$	−0.59645	0.08439	0.08242,[g] 0.08200,[h] 0.08200[i]	0.08198
$6s6p\ ^3P_2$	−0.58914	0.09170	0.09038,[g] 0.08999,[h] 0.09002[i]	0.08981
$6s5d\ ^3D_1$	−0.56110	0.11973	0.11362,[g] 0.11425,[h] 0.11158[i]	0.11158
$6s5d\ ^3D_2$	−0.55975	0.12109	0.11473,[g] 0.11136,[h] 0.11274[i]	0.11278
$6s5d\ ^3D_3$	−0.55602	0.12481	0.11699,[g] 0.11503,[h] 0.11517[i]	0.11514
$6s6p\ ^1P_1$	−0.55301	0.12782	0.12426,[g] 0.11253,[h] 0.11669[i]	0.11422
$6s5d\ ^1D_2$	−0.54667	0.13416	0.13025,[g] 0.12595,[h] 0.12672[i]	0.12611

[a]Reference [61].
[b]Reference [62].
[c]Reference [60].
[d]Reference [64].
[e]Reference [66].
[f]Reference [30].
[g]Reference [19].
[h]Reference [67].
[i]Reference [68].

[62]. Previous works of Eliav, Kaldor, and Ishikawa [19,64] reported the excited energy calculations of atomic Ba and Yb using the Fock-space-based coupled-cluster theory. The other widely used atomic many-body method employed is configuration-interaction MBPT (CI-MBPT) [65], based on Dzuba and Ginges [30] calculated the excitation energies of Ba. Same method was used by Porsev and collaborators to calculate the excitation energies and HFS constants of Yb [67].

One reason for choosing the three atoms in our calculations is the significant difference in the sequences of $ns(n-1)d\ ^3D_J$, $ns(n-1)d\ ^1D_2$, $nsnp\ ^3P_J$, and $nsnp\ ^1P_1$ levels. As evident from Table I, in Sr the $5s4d\ ^{2S+1}D_J$ levels lie between $5s5p\ ^3P_J$ and $5s5p\ ^1P_1$, whereas the $6s5d\ ^{2S+1}D_J$ levels are

below the $6s6p\ ^{2S+1}P_J$ levels in Ba. The difference in the level structure can be attributed to the presence of an additional diffuse shell $4d$. The sequence gets more complicated in Yb,

TABLE II. The nuclear spin I, the magnetic moment μ (in nuclear magneton), and the electric quadrupole moment Q (in barn), used in the paper.

Ion	I	μ	Q
^{87}Sr	9/2	−1.0936(13)	+0.305
^{137}Ba	3/2	+0.93737(2)	+0.246(2)
^{173}Yb	5/2	−0.648(3)	+2.80(4)

TABLE III. The magnetic dipole HFS constant for ^{173}Yb$^+$ and the electric quadrupole HFS constant for ^{87}Sr$^+$, ^{137}Ba$^+$, and ^{173}Yb$^+$ ions. All the values are in MHz.

Ion	State	This work	Other works	Experiment
		Magnetic dipole HFS constant A		
^{173}Yb$^+$	$6s_{1/2}$	−3529.660	−3507[a]	−3497.5(6)[a], −3508(9)[c]
	$6p_{1/2}$	−612.362	−638[a]	−518.2(4)[a], −600[c]
	$6p_{3/2}$	−88.973	−107[a]	–
	$5d_{3/2}$	−104.479	−110.31[b]	–
	$5d_{5/2}$	22.078	3.47[b]	–
		Electric quadrupole HFS constant B		
^{87}Sr$^+$	$5p_{3/2}$	84.806	82.655,[d] 83.662[e]	88.5(5.4)[g]
	$4d_{3/2}$	33.961	35.075,[d] 36.051,[e] 39.60[b]	–
	$4d_{5/2}$	48.055	48.800,[d] 51.698,[e] 56.451[b] 49.166[f]	49.11(6)[h]
^{137}Ba$^+$	$6p_{3/2}$	98.954	92.275[i]	92.5(0.2)[j]
	$5d_{3/2}$	45.765	51.32,[b] 47.3,[k] 46.82[i]	44.541(17)[k]
	$5d_{5/2}$	62.685	68.16,[b] 63.2,[k] 62.27[i]	59.533(43),[k] 60.7(10),[l] 62.5(40)[m]
^{173}Yb$^+$	$6p_{3/2}$	1839.779	1780[a]	1460(50)[n]
	$5d_{3/2}$	902.301	951.4[b]	–
	$5d_{5/2}$	1165.046	1190.4[b]	–

[a]Reference [71].
[b]Reference [72].
[c]Reference [73].
[d]Reference [74].
[e]Reference [75].
[f]Reference [76].
[g]Reference [77].
[h]Reference [38].
[i]Reference [78].
[j]Reference [79].
[k]Reference [80].
[l]Reference [81].
[m]Reference [82].
[n]Reference [83].

$6s6p\ ^3P_J$ levels are below $6s5d\ ^3D_J$, however, the $6s6p\ ^1P_1$ lies between $6s5d\ ^3D_2$ and $6s5d\ ^3D_3$. It is to be noted that the difference between Ba and Yb configurations is the presence of $4f$ in the Yb core and is the cause for the change in the level sequence.

The excitation energies obtained from our calculations are reasonably close to the other theoretical results for Sr and Ba. However, there is a lack of clear trend in the differences. For the excitation energies of Sr, our results are consistently better than the MCHF results [60], and our result of $5s5p\ ^3P_2$ is closest to the experimental value. One observation is, although Porsev and collaborators [61], and Savukov and Johnson [62] used the same method CI-MBPT, the results from the former are consistently better than the latter. A possible reason could be the single-particle basis set. The former used a combination of V^N, V^{N-1}, and V^{N-2} orbitals for the core and valence, and virtuals are generated through a recurrent procedure. In the later work, the orbital sets are B splines. As described earlier, we use numerical Gaussian-type orbitals for our calculations.

A comparison of excitation energies of Ba presents an interesting case. Some of our results are better than the previous CC results of Eliav and collaborators [64]. The results provide a numerical validation of our approach. On the other hand, the results of Dzuba and collaborators [65] and Safronova and collaborators [66] use similar basis sets but different many-body methods. The former used CI-MBPT, whereas the latter used the recently developed CI plus all order method [66]. The results from the latter are consistently better than the former.

The Yb excitation energy calculations presents a serious challenge. Earlier CC calculations of Yb excitation energies [19] could not reproduce the experimental sequence and we also encounter the same issue. In particular, the $6s6p\ ^1P_1$ is above the $6s5d\ ^3D_J$ levels, whereas experimentally it lies between $6s5d\ ^3D_2$ and $6s5d\ ^3D_3$. Sequence in our results is similar and individual values are consistently higher than the previous CC calculations. The sequence, however, is correctly reproduced in another calculation with the CI-MBPT method [67], where the basis set used is a combination of Dirac-Fock orbitals for the core and valence, and virtuals are generated through recurrent procedure. The comparison of the different results indicate a wide variation in the many-body methods and single-particle states. In fact, none of the works listed and referred have a common many-body theory and basis sets. Perhaps, this is an indication of the issues which

TABLE IV. Magnetic dipole and electric quadrupole HFS constants contributions from different terms.

Ion	State	Coupled-cluster terms							Other terms	Norm
		DF	$\tilde{H}_{\text{hfs}}$-DF	$S^{\dagger}\tilde{H}_{\text{hfs}} + \text{c.c.}$	$S_2^{\dagger}\tilde{H}_{\text{hfs}}S_1 + \text{c.c.}$	$S_1^{\dagger}\tilde{H}_{\text{hfs}}S_1$	$S_2^{\dagger}\tilde{H}_{\text{hfs}}S_2$			
				HFS constant A						
^{173}Yb$^+$	$6s_{1/2}$	−2582.096	130.175	−998.855	−31.463	−48.566	−60.815	14.667	1.013
	$6p_{1/2}$	−408.696	15.693	−197.323	−7.054	−10.972	−6.151	−4.378	1.011
	$6p_{3/2}$	−48.278	1.798	−32.418	−1.817	−1.234	−7.445	−0.591	1.011
	$5d_{3/2}$	−75.876	0.192	−19.903	−0.870	−1.289	−8.127	−0.122	1.015
	$5d_{5/2}$	−28.899	−0.536	52.927	4.081	−0.424	−4.903	0.082	1.011
				HFS constant B/Q						
^{87}Sr$^+$	$6p_{3/2}$	166.993	−2.509	109.511	4.024	2.565	7.769	−2.302	1.001
	$5d_{3/2}$	80.939	7.879	26.888	−.573	1.073	−3.540	−0.791	1.005
	$5d_{5/2}$	110.863	15.702	34.180	−.848	1.377	−1.911	−1.081	1.005
^{137}Ba$^+$	$6p_{3/2}$	229.303	−5.962	170.985	7.425	5.364	−1.153	−3.097	1.002
	$5d_{3/2}$	135.098	12.635	46.886	.211	1.305	−7.849	−1.213	1.006
	$5d_{5/2}$	172.975	25.621	63.015	.333	1.627	−5.898	−1.508	1.005
^{173}Yb$^+$	$6p_{3/2}$	372.894	−16.855	274.025	11.547	9.994	−0.212	6.441	1.001
	$5d_{3/2}$	199.032	11.143	112.382	1.292	3.058	−4.128	0.975	1.005
	$5d_{5/2}$	234.438	21.220	152.106	2.217	3.080	4.774	−0.041	1.004

require consistent efforts to resolve the difficulties of precision calculations of two-valence systems.

B. Hyperfine structure constants

Hyperfine constants are appropriate atomic properties to inspect the accuracy of atomic wave functions in the small radial distances—within and close to the nucleus. For the calculations we use the nuclear moments given in the compilation of Stone [69] and the values are given Table II.

1. Hyperfine constant A of Yb$^+$

The magnetic dipole HFS constant of ^{173}Yb$^+$ and the electric quadrupole HFS constants of ^{87}Sr$^+$, ^{137}Ba$^+$, and ^{173}Yb$^+$ from our calculations are given in Table III. For comparison, the results from other theoretical studies and experimental data are also given. Contributions from the specific terms in the CC properties expression of HFS are listed in Table IV. Previous theoretical study by Martensson [71] on the magnetic dipole HFS constant of ^{173}Yb$^+$ is based on the CCT and basis set is obtained from discrete spectrum method [70]. In this work, the HFS constant a of $6s_{1/2}$, $6p_{1/2}$, and $6p_{3/2}$ are calculated. Our result of $6s_{1/2}$ is slightly higher than both the theoretical and experimental values. However, for $6p_{1/2}$ our result is lower than the previous theoretical result of Martensson [71] and closer to the experimental data [71]. Similarly, our result of $6p_{3/2}$ is lower than the value of Martensson [71]. Although, the many-body methods employed in the two calculations are same; HFS constants of p in our results are lower. Coming to the $5d$ states, the previous calculations of Itano is based on multiconfiguration Dirac-Fock (MCDF) [58]. The $5d_{3/2}$ results are close to our value, however, for the $5d_{5/2}$ state our results are much larger. At this stage it is difficult to pinpoint the reason for the large discrepancy between the two results. One observation from the component-wise contribution in Table IV is the

large cancellation between the Dirac-Fock (leading order) and the next to leading order ($S^{\dagger}\tilde{H}_{\text{hfs}} + \text{c.c.}$). Similar pattern is observed in the HFS constant of $nd_{5/2}$ state of all the alkaline-earth-metal ions reported in our previous work [18]. A comparison shows the cancellation is larger in Yb$^+$. Another notable difference in Yb$^+$ is that the ($S_2^{\dagger}\tilde{H}S_1 + \text{c.c.}$) is large and almost cancels with $S_2^{\dagger}\tilde{H}S_2$.

2. Hyperfine structure constant b of p$_{3/2}$ states

Leading terms, listed in Table IV, are the Dirac-Fock and ($S^{\dagger}\tilde{H}_{\text{hfs}} + \text{c.c.}$). The later subsumes the core-polarization effects. For all the ions, Sr$^+$, Ba$^+$, and YB$^+$, the contributions from these two terms are almost equal. This is a significant deviation from the observed pattern in the magnetic dipole HFS constant [18], which noticeable for Yb$^+$ in Table IV. Among all the theoretical calculations our results for Sr$^+$ is in better agreement with the experimental data. For Ba$^+$, no previous theoretical works and experimental data are available. Ours is the first study on the electric quadrupole HFS constant of the $6p_{3/2}$ state. Our result of Yb$^+$ is higher than the previous theoretical results of Martensson-Pendrill and collaborators [71] as well as the experimental results of Berends and Maleki [83].

3. Hyperfine structure constant B of d states

The HFS constant B_d of Sr$^+$ has been studied in several theoretical works. Our results of B are systematically lower than the other theoretical values, which is evident from Table III. The previous calculations of Martensson [74] used the same many-body method like ours, relativistic coupled cluster, but a different type of single-particle basis set. The calculations of Sahoo [76], in terms of theoretical methods, are closest to ours. They have used the relativistic coupled-cluster and Gaussian-type basis set like we have done. However, Sahoo calculated only for the $4d_{5/2}$ state and his result is

TABLE V. Magnetic dipole HFS constant for the atomic systems ^{87}Sr, ^{137}Ba, and ^{173}Yb, using relativistic coupled-cluster theory. All values are in atomic units.

State	Coupled-cluster terms					Other work	Expt. result
	DF	$\tilde{H}_{hfs}$-DF	One-body $\tilde{H}_{hfs}$	Two-body $\tilde{H}_{hfs}$	Total value		
Atomic ^{87}Sr; [Kr]$5s^2$							
$5s5p\ ^3P_1$	−178.983	−0.120	−49.121	0.002	−228.222	–	−260.765(1)[j]
$5s5p\ ^3P_2$	−200.670	0.106	−47.045	0.002	−247.607	–	−212.085(5)[j]
$5s4d\ ^3D_1$	145.335	0.098	6.348	0.001	151.586	–	–
$5s4d\ ^3D_2$	−56.824	0.076	7.095	0.001	−49.654	–	–
$5s4d\ ^3D_3$	−133.930	−0.040	0.194	0.002	−133.778	–	–
$5s4d\ ^1D_2$	17.441	0.062	9.643	0.001	27.145	–	–
$5s4d\ ^1P_1$	11.802	−0.225	4.366	−0.002	15.941	–	–
Atomic ^{137}Ba; [Xe]$6s^2$							
$6s5d\ ^3D_1$	−588.432	0.344	−19.420	−0.004	−607.512	−547[a]	−521[c]
$6s5d\ ^3D_2$	397.451	−0.588	9.067	−0.009	405.921	405[a]	416[c]
$6s5d\ ^3D_3$	543.921	0.189	4.843	−0.008	548.945	443[a]	457[c]
$6s5d\ ^1D_2$	−148.545	−0.459	−54.967	−0.006	−203.977	−102[a]	−82[d]
$6s6p\ ^3P_1$	736.066	−0.310	221.943	−0.004	957.695	1160[a]	1151[e]
$6s6p\ ^3P_2$	806.032	−0.152	204.186	−0.010	1010.056	845[a]	–
$6s6p\ ^1P_1$	−181.658	−0.074	−38.353	0.009	−220.094	−107[a]	−109[f]
Atomic ^{173}Yb; [Xe]$4f^{14}6s^2$							
$6s6p\ ^3P_1$	−708.922	−0.223	−197.665	0.004	−906.806	−1094[b]	−1094.2(6)[g]
$6s6p\ ^3P_2$	−681.732	−0.292	−181.832	0.003	−863.853	−745[b]	−738[h]
$6s5d\ ^3D_1$	550.679	0.035	64.941	0.002	615.657	596[b]	563(1)[i]
$6s5d\ ^3D_2$	−456.152	−0.064	−40.287	0.003	−496.500	−351[b]	−362(2)[i]
$6s5d\ ^3D_3$	−454.431	−0.027	−22.482	0.002	−476.938	−420[b]	−430(1)[i]
$6s6p\ ^1P_1$	239.530	0.499	65.911	−0.002	305.938	191[b]	60[h]
$6s5d\ ^1D_2$	197.218	−0.011	71.840	0.002	269.049	131[b]	100(18)[i]

[a]Reference [84].
[b]Reference [67].
[c]Reference [85].
[d]Reference [86].
[e]Reference [87].
[f]Reference [88].
[g]Reference [89].
[h]Reference [90].
[i]Reference [91].
[j]Reference [92].

closest to the experimental data. Ours on the other hand is ≈2.3% lower than his result. Similarly, for the same reasons for the HFS constants B of Ba$^+$, the previous calculations of Sahoo [78] is closest to ours. However, our result of $5d_{3/2}$ is closer to the experimental data. For $5d_{5/2}$ state our value is ≈0.6% lower than the theoretical value of Sahoo and ≈5.3% higher than the experimental value. Considering that for the Sr$^+$ and Ba$^+$ calculations, the many-body method and type of single-particle basis we have used are the same as in Refs. [76] and [78], respectively. The difference in the results could be on account of minor differences in the exponents used in the basis set generation or the truncation of the coupled-cluster properties expression. There are striking changes, when compared with the $p_{3/2}$, in the component-wise contribution. Dirac-Fock contributions in both Sr$^+$ and Ba$^+$ are approximately three times larger than $(S^\dagger \tilde{H}_{hfs} + c.c..$ In addition, the contribution from the $\tilde{H}_{hfs}$-DF, which essentially arises from the closed-shell part, is relatively large. This could

be due to the diffuse electron density of the d orbitals and hence stronger interaction with the core electrons.

Unlike the other two ions, Yb$^+$ has not been studied in fine detail. The previous theoretical work of Itano [72] is based on the MCDF method. And there are no experimental data available for the ^{173}Yb$^+$ isotope. Our results are lower but close to the values from Itano [72]. A closer inspection of the results from Itano's calculations for the other ions (Sr$^+$ and Ba$^+$) reveals that his results are consistently higher than the other theoretical and experimental data. One possible reason could be the contracted nature of the virtual orbitals, referred to as correlation orbitals, in MCDF calculations. Hence, we can expect a similar trend in Yb$^+$ as well and it is possible that our results are closer to the actual values. Compared to Sr$^+$ and Ba$^+$, there is one remarkable change in the component-wise contribution. There is large contribution from $(S^\dagger \tilde{H}_{hfs} + c.c.)$, which implies that their core-polarization effect is very important. It is on par with the Dirac-Fock term.

TABLE VI. Magnitude of the electric dipole transition amplitude for ^{87}Sr$^+$, ^{137}Ba$^+$, and ^{173}Yb$^+$ ions.

Ion	Transition	This work	Other works
^{87}Sr$^+$	$5p_{1/2} \longrightarrow 5s_{1/2}$	3.2180	3.060[a]
	$5p_{3/2} \longrightarrow 5s_{1/2}$	4.9223	4.325[a]
	$5p_{1/2} \longrightarrow 4d_{3/2}$	3.4315	3.052[a]
	$5p_{3/2} \longrightarrow 4d_{3/2}$	1.4217	1.355[a]
	$5p_{3/2} \longrightarrow 4d_{5/2}$	4.5942	4.109[a]
^{137}Ba$^+$	$6p_{1/2} \longrightarrow 6s_{1/2}$	3.1974	3.300,[a] 3.36(1),[b] 3.272[c]
	$6p_{3/2} \longrightarrow 6s_{1/2}$	5.0330	4.658,[a] 4.73(3),[b] 4.614[c]
	$6p_{1/2} \longrightarrow 5d_{3/2}$	3.0898	3.009,[a] 3.11(3),[b] 3.008[c]
	$6p_{3/2} \longrightarrow 5d_{3/2}$	1.2448	1.312,[a] 1.34(2),[b] 1.313[c]
	$6p_{3/2} \longrightarrow 5d_{5/2}$	4.1347	4.057,[a] 4.02(7),[b] 4.054[c]
^{173}Yb$^+$	$6p_{1/2} \longrightarrow 6s_{1/2}$	2.9069	2.731[d]
	$6p_{3/2} \longrightarrow 6s_{1/2}$	4.5256	3.845[d]
	$6p_{1/2} \longrightarrow 5d_{3/2}$	3.6317	3.782[d]
	$6p_{3/2} \longrightarrow 5d_{3/2}$	1.4918	1.546[d]
	$6p_{3/2} \longrightarrow 5d_{5/2}$	4.8500	4.769[d]

[a]Reference [93].
[b]Reference [12].
[c]Reference [94].
[d]Reference [95].

4. HFS of two-valence systems

There are few theoretical and experimental works on the HFS constants of the neutral alkaline-earth-metal atoms and Yb. However, the importance of such investigations is likely to grow in the near future as these, in particular Sr and Yb, are candidates of precision experiments and have been cooled to quantum degeneracy. In our work we make an effort to understand the systematics to initiate a deeper analysis on the role of the electron correlation effects to properties like hyperfine. The previous theoretical calculations of ^{137}Ba [84] and ^{173}Yb [67] are based on the CI-MBPT method and basis

with different central potentials. For this reason it is nontrivial to comment on the role of the correlation effects in a precise manner through a comparative study. The results from our calculations, along with the leading order contributions, are listed in Table V. From the table it is clear that, in most of the cases, our theoretical results are not in very good agreement with the experimental data. Origin of the discrepancy could be the nature of the single-particle basis we have used, the V^{N-2} orbitals. On account of the doubly ionized charged state of the core, the orbitals are highly contracted and interact rather strongly with the nucleus. Such orbitals are suitable for

TABLE VII. The electric dipole transition amplitude, contributions from different terms in the coupled-cluster theory.

Ion	Transition	Coupled-cluster terms						Other terms	Norm
		DF	$\tilde{D}$-DF	$S^\dagger \tilde{D}$ + c.c.	$S_2^\dagger \tilde{D} S_1$ + c.c.	$S_1^\dagger \tilde{D} S_1$	$S_2^\dagger \tilde{D} S_2$		
^{87}Sr$^+$	$5p_{1/2} \longrightarrow 5s_{1/2}$	3.4869	0.0008	-0.2715	-0.0043	0.0129	0.0233	-0.0004	0.9909
	$5p_{3/2} \longrightarrow 5s_{1/2}$	4.9246	0.0019	-0.0072	$-0.0003.1$	0.0187	0.0034	-0.0047	0.9902
	$5p_{1/2} \longrightarrow 4d_{3/2}$	3.7226	0.0024	0.2902	-0.0062	0.0178	0.0234	0.0031	0.9889
	$5p_{3/2} \longrightarrow 4d_{3/2}$	1.6543	0.0001	-0.2332	-0.0028	0.0080	0.0122	0.0002	0.9882
	$5p_{3/2} \longrightarrow 4d_{5/2}$	-4.9937	-0.0005	0.3967	0.0085	-0.0238	-0.0334	-0.0006	0.9887
^{137}Ba$^+$	$6p_{1/2} \longrightarrow 6s_{1/2}$	3.8911	0.0019	-0.7618	-0.0097	0.0442	0.0715	-0.0009	0.9880
	$6p_{3/2} \longrightarrow 6s_{1/2}$	-5.4778	-0.0046	0.5275	0.0134	-0.0609	-0.0973	0.0014	0.9872
	$6p_{1/2} \longrightarrow 5d_{3/2}$	-3.7450	-0.0080	0.7220	-0.0001	-0.0392	-0.0685	0.0008	0.9846
	$6p_{3/2} \longrightarrow 5d_{3/2}$	1.6352	0.0119	-0.4240	0.0005	0.0161	0.0363	0.0000	0.9838
	$6p_{3/2} \longrightarrow 5d_{5/2}$	5.0005	0.0102	-0.9544	0.0011	0.0485	0.0930	-0.0001	0.9847
^{173}Yb$^+$	$6p_{1/2} \longrightarrow 6s_{1/2}$	3.2422	0.0011	-0.3387	-0.0071	0.0181	0.0247	0.0043	0.9872
	$6p_{3/2} \longrightarrow 6s_{1/2}$	-4.5426	-0.0032	0.0282	-0.0001	-0.0231	-0.0430	-0.0021	0.9868
	$6p_{1/2} \longrightarrow 5d_{3/2}$	-3.8611	-0.0024	0.2336	0.0095	-0.0286	-0.0366	0.0055	0.9869
	$6p_{3/2} \longrightarrow 5d_{3/2}$	.6970	0.0002	-0.2551	-0.0039	0.0114	0.0165	-0.0022	0.9865
	$6p_{3/2} \longrightarrow 5d_{5/2}$	-5.2002	0.0008	0.3448	0.0117	-0.0325	-0.0443	0.0113	0.9881

TABLE VIII. E1 transition amplitudes for the atomic system ^{87}Sr, using relativistic coupled-cluster theory. All values are in atomic units.

| Transition | Coupled-cluster terms | | | | | Other work |
	DF	$\tilde{H}_{\text{hfs}}$-DF	One-body $\tilde{H}_{\text{hfs}}$	Two-body $\tilde{H}_{\text{hfs}}$	Total value	
$^3P_1 \longrightarrow {}^1S_0$	-0.3759	-0.0001	0.8257	0.00001	0.4497	$0.16,^a$ 0.162^b
$^1P_1 \longrightarrow {}^1S_0$	-4.2442	0.0000	0.5283	-0.00002	-3.7159	$5.28,^a$ $5.238,^b$ 1.9539^c
$^3P_0 \longrightarrow {}^3D_1$	2.6323	-0.0002	-0.3131	0.00000	2.3190	
$^3P_1 \longrightarrow {}^3D_1$	2.2652	0.0013	0.1116	0.00000	2.3781	
$^3P_2 \longrightarrow {}^3D_1$	0.5849	0.0009	0.3772	-0.00001	0.9630	
$^1P_1 \longrightarrow {}^3D_1$	0.2255	-0.0005	-0.2496	-0.00001	-0.0247	
$^3P_1 \longrightarrow {}^3D_2$	3.9538	0.0012	-0.5437	-0.00001	3.4114	
$^3P_2 \longrightarrow {}^3D_2$	2.2646	0.0006	0.0700	0.00001	2.3352	
$^1P_1 \longrightarrow {}^3D_2$	0.7531	-0.0004	-0.1054	0.00001	0.6473	
$^3P_2 \longrightarrow {}^3D_3$	-5.3938	-0.0001	0.3111	0.00001	-5.0828	
$^3P_1 \longrightarrow {}^1D_2$	-0.8822	0.0012	0.0387	0.00000	-0.8423	0.19^a
$^3P_2 \longrightarrow {}^1D_2$	-0.2854	0.0002	-0.3597	-0.00001	-0.6448	0.10^a
$^1P_1 \longrightarrow {}^1D_2$	-4.5484	-0.0008	0.3860	-0.00001	-4.1632	1.92^a

^{a}Reference [61].
^{b}Reference [62].
^{c}Reference [60].

properties calculations of singly ionized states but not ideal for the neutral atoms.

A very important aspect of our present work is the observed trend in the contributions from various terms. It is evident from Table V the DF contribution is significantly dominant; it is far larger than the next to leading order contribution from what we refer to as the *one-body terms*. The details of the *one-body terms* are discussed in Sec. V C 1. To quantify the relative contributions, define

$$\varrho = \frac{\text{one-body terms}}{\text{DF}}, \qquad (75)$$

essentially the ratio between the leading and next to leading order contributions. The dominance of DF is particularly true in the case of the $ns(n-1)d\ ^3D_J$ states, among these states highest ϱ is ≈ 0.12 ($5s4d\ ^3D_2$ state of ^{87}Sr). For the $nsnp\ ^3P_J$ states, the contribution from the *one-body terms* is small but not

negligible. Largest and smallest value of ϱ for these states are ≈ 0.3 for the $6s6p\ ^3P_1$ state of Ba and ≈ 0.23 for the $5s5p\ ^3P_2$ state of Sr, respectively. Other states have ϱ close to 0.25.

For the singlet states $nsnp\ ^1P_1$ and $ns(n-1)d\ ^1D_2$, the deviations from the experimental data are very large. A similar trend was also observed in the case of the excitation energy of these states as well.

C. E1 transition amplitude

We calculate the reduced matrix element of the dipole operator **D** from the expression given in Eq. (59). Once again, like in the HFS constants, we calculate the reduced matrix elements of the Sr$^+$, Ba$^+$, and Yb$^+$ ions from the intermediate one-valence wave functions. In the present work, we do not attempt to quantify the error or accuracy of the results. This is a work in progress and we shall report in our future publications

TABLE IX. E1 transition amplitudes for the atomic system ^{137}Ba, using relativistic coupled-cluster theory. All values are in atomic units.

| Transition | Coupled-cluster terms | | | | | Other work |
	DF	$\tilde{H}_{\text{hfs}}$-DF	One-body $\tilde{H}_{\text{hfs}}$	Two-body $\tilde{H}_{\text{hfs}}$	Total value	
$^3P_1 \longrightarrow {}^1S_0$	0.3888	-0.0003	-0.8090	0.00000	0.4205	0.4537^a
$^1P_1 \longrightarrow {}^1S_0$	-4.6768	-0.0002	0.6730	0.00000	4.0040	5.236^a
$^3P_0 \longrightarrow {}^3D_1$	2.6203	0.0004	-0.2585	0.00000	2.3622	2.3121^a
$^3P_1 \longrightarrow {}^3D_1$	2.2405	-0.0023	-0.0195	0.00000	2.2187	2.0108^a
$^3P_2 \longrightarrow {}^3D_1$	-0.5715	0.0019	-0.4782	0.00000	1.0478	0.5275^a
$^1P_1 \longrightarrow {}^3D_1$	-0.3364	-0.0002	0.3546	0.00000	0.0180	0.1047^a
$^3P_1 \longrightarrow {}^3D_2$	3.8886	-0.0022	-0.1585	0.00001	3.7279	3.4425^a
$^3P_2 \longrightarrow {}^3D_2$	-2.2265	0.0013	0.1007	-0.00001	2.1245	2.024^a
$^1P_1 \longrightarrow {}^3D_2$	-0.3874	-0.0005	0.0833	-0.00000	0.3046	0.4827^a
$^3P_2 \longrightarrow {}^3D_3$	5.3410	-0.0004	-0.3409	-0.00001	4.9997	4.777^a
$^3P_1 \longrightarrow {}^1D_2$	-1.1039	-0.0018	0.1178	0.00000	0.9879	0.1610^a
$^3P_2 \longrightarrow {}^1D_2$	0.4458	0.0005	0.5219	0.00001	0.9682	0.1573^a
$^1P_1 \longrightarrow {}^1D_2$	4.4933	-0.0011	-0.0773	0.00000	4.4149	1.047^a

^{a}Reference [30].

TABLE X. E1 transition amplitudes for the atomic system ^{173}Yb, using relativistic coupled-cluster theory. All values are in atomic units.

Transition	Coupled-cluster terms					Other work
	DF	$\tilde{H}_{hfs}$-DF	One-body $\tilde{H}_{hfs}$	Two-body $\tilde{H}_{hfs}$	Total value	
$^3P_1 \longrightarrow\ ^1S_0$	0.1445	−0.0003	−0.5320	0.00000	−0.3878	0.54(8),[a] 0.44,[b] 0.587[c]
$^1P_1 \longrightarrow\ ^1S_0$	−3.8641	−0.0001	0.5999	−0.00001	−3.2643	4.40(80),[a] 4.44,[b] 4.89,[d] 4.825[c]
$^3P_0 \longrightarrow\ ^3D_1$	2.7296	0.0001	−0.3209	0.00000	2.4088	2.61(10),[a] 2.911[c]
$^3P_1 \longrightarrow\ ^3D_1$	2.3473	−0.0005	0.1811	0.00003	2.5279	2.26(10)[a]
$^3P_2 \longrightarrow\ ^3D_1$	−0.5997	0.0000	−0.2343	0.000002	−0.8340	0.60(12)[a]
$^1P_1 \longrightarrow\ ^3D_1$	−0.4503	−0.0002	0.1702	0.00000	−0.2803	0.27(10),[a] 0.24[b]
$^3P_1 \longrightarrow\ ^3D_2$	3.9875	−0.0005	−0.6480	0.00002	3.3390	4.03(16)[a]
$^3P_2 \longrightarrow\ ^3D_2$	−2.2940	−0.0002	−0.1010	−0.00003	−2.3952	2.39(1)[a]
$^1P_1 \longrightarrow\ ^3D_2$	0.0716	−0.0003	0.0660	0.00000	0.1373	0.32(6),[a] 0.60[b]
$^3P_2 \longrightarrow\ ^3D_3$	5.6130	0.0000	−0.3215	−0.00001	5.2915	6.12(30)[a]
$^3P_1 \longrightarrow\ ^1D_2$	−1.1920	−0.0006	0.0995	0.00000	−1.0931	0.54(10)[a]
$^3P_2 \longrightarrow\ ^1D_2$	0.5946	0.0002	0.3601	0.00000	0.9549	0.38(8)[a]
$^1P_1 \longrightarrow\ ^1D_2$	4.7006	−0.0002	−0.5209	0.00000	4.1795	3.60(70)[a]

[a]Reference [96].
[b]Reference [97].
[c]Reference [68].
[d]Reference [98].

with a careful examination of the different types of basis functions, and calculate the dipole matrix elements in different gauges.

1. One-valence

Results from our calculations are listed in Table VI and component-wise contributions are given in Table VII. One of the early works on the dipole matrix elements of singly ionized alkaline-earth-metal ions is by Guet and Johnson [93]. The many-body methods they used are MBPT and random-phase approximation (RPA), and numerical basis set. At the DF level the values of Guet and Johnson [93] are in good agreement, for both Sr$^+$ and Ba$^+$, with our results; this is evident from the values listed in Table VII. Their work is the only one in the literature on the electric dipole matrix elements of Sr$^+$ and our results are higher. The difference could be largely attributed to the higher order core-polarization effects associated with the random-phase approximation. The RPA effects are incorporated in the coupled cluster but not to higher order as in an iterative RPA calculation.

For Ba$^+$ there are several theoretical calculations of the electric dipole matrix elements. A careful study on the electric dipole transition is desirable as it a promising candidate for a novel parity nonconservation experiment [41]. In terms of the many-body method and single-particle basis set, the calculations of Sahoo and collaborators [12] are closest to our approach. They estimate the upper bound on the error in the reduced dipole matrix element as 1.7%, which implies that our results have errors larger than this.

For Yb$^+$, the work of Safronova and Safronova [95] is the only previous study on the electric dipole matrix elements. Their calculations are based on the third-order relativistic MBPT and the excellent matching between the length and velocity gauge results indicates the results are quite accurate.

Our results are close to their results, however, at this stage we do not attempt to estimate the accuracy of our results.

2. Two-valence

Our results of the dipole matrix elements of Sr, Ba, and Yb are listed in Tables VIII–X. There are very few theoretical studies on the dipole matrix elements of Sr and those are not in very good agreement with ours. In the case of Ba, the previous theoretical calculations were done by Dzuba and Ginges [30]. Our results, listed in Table IX, are in good agreement with Ref. [30] for the $\langle 6s6p\ ^3D_1||D||6s^2\ ^1S_0 \rangle$ and $\langle 6s6p\ ^3D_J||D||6s5d\ ^3D_J \rangle$. However, there are large deviations for the matrix elements involving the $6s6p\ ^1P_1$ and $6s5d\ ^1D_2$ states. For Yb, the $\langle 6s6p\ ^1P_1||D||6s5d\ ^3D_2 \rangle$ is significantly different from the previous results. However, there is a large difference between the previous results of Porsev and collaborators [96], and Migdalek and Baylis [97] as well. Large relative deviations, compared to results of Ref. [96], are also observed for the $\langle 6s6p\ ^3P_1||D||6s5d\ ^1D_2 \rangle$ and $\langle 6s6p\ ^3P_2||D||6s5d\ ^1D_2 \rangle$.

VIII. CONCLUSIONS

In this paper we describe in detail the Fock-space relativistic coupled-cluster method for the two-valence systems. It is based on an all-particle treatment and we demonstrate the excitation energies of Ba and Yb are on par with those of the previous relativistic CC calculations. The key point is that we have implemented the Fock-space CCT with an incomplete but quasicomplete model space comprising the ns^2, $ns(n-1)d$, and $nsnp$ configurations. This choice of model space is optimal to study the low-lying states of the alkaline-earth-metal atoms and other two-valence atoms like Yb and Hg. Most importantly, with this model space one may avoid divergences arising from the *intruder* states. This ought to be highlighted as the literature on iterative studies of two-valence systems,

replete with accounts of *intruder*-state-induced divergences. We emphasize that there are few detailed relativistic many-body calculations of two-valence excitation energies and even less on properties calculations. Not surprisingly, among the published results there is a wide variation of the many-body methods and basis sets used in the studies. Considering the growing importance of alkaline-earth-metal atoms in precision experiments and possible applications, a detailed investigations on the two-valence systems is timely.

We have also developed a method based on CCT to compute properties from the CC wave functions of two-valence systems. This is perhaps an initial step toward systematic investigation of the structure and properties of two-valence systems with CCT, which has not been attempted before. Based on our scheme, the computational cost of two-valence CC calculations is marginally higher than the one-valence calculations. And the additional cost is in solving the $S^{(2)}$ cluster amplitude equations, the total number of which is far less than the closed-shell and one-valence cluster amplitudes T and $S^{(1)}$, respectively. So in terms of computational implementations, there is no reason why two-valence CCT should not be the preferred method as in one-valence systems. The important and essential details of our schemes and implementations are provided to highlight important physics issues in the two-valence Fock-space CCT. Brief descriptions of the method and extensive references are provided to aid interested researchers to implement CCT of two-valence systems.

From the many-body theory perspective, CCT-based structure and properties calculations is certainly an attractive choice, the prime reason being that the topologically connected nature of the CC operators and the exponential form of the wave operator ensures the condition of size extensivity, a basic requirement of a legitimate many-body theory. Furthermore, the nonperturbative character of the CC wave operator makes it an ideal choice. It must be emphasized that all of these considerations are at the level of the many-body theory. However, the accuracy of the results also depends on other factors like single-particle basis set considered.

In the method we have developed, the one-valence coupled-cluster wave functions occur as an intermediate step. Using this we calculate the electric quadrupole HFS constant B of Sr^+, Ba^+, and Yb^+. The HFS constant B of the $5p_{3/2}$ $^2P_{3/2}$ and $5d_{3/2}$ $^2D_{3/2}$ states of $^{87}Sr^+$ and $^{137}Ba^+$, respectively, are closer to the experimental data than the other theoretical results. For all the ions studied, the $np_{3/2}$ $^2P_{3/2}$ state has very large contributions from the core polarization effects, which is part of $(S^\dagger \tilde{H}_{hfs} + c.c.)$ in the CC properties calculations. Similaraly, for $5d_j$ ^2D_j states of Yb^+, there is a large contribution from the core-polarization effects. A careful accounting of the core-polarization effects is crucial for all the ions to obtain

accurate values of B and this is particularly true for Yb^+. We also calculate the magnetic dipole HFS constant A of Yb^+; except for the $5d_{5/2}$ state the results are in agreement with the other theoretical and experimental data. Similarly, we get reliable results of the dipole matrix elements of these ions.

The results of the excitation energies of the two-valence sector calculations are in agreement with the previous CC results. For properties calculations with CC wave functions, our results show deviations from the previous works. However, it must be mentioned that there have been very few attempts at theoretical properties calculations of two-valence systems. And the previous works are based on MCDF or using a collage of single-particle wave functions. The latter may require finer analysis for precision studies as the linked-cluster theorem, which forms the basis of many-body theory, is based on a uniform separation of the total Hamiltonian into zeroth order and perturbation. This is not the case when orbitals with different central potentials are used in the calculations. With the MCDF method, a large-scale structure and properties calculations of neutral atoms with high Z is plagued with convergence issues. Among all the states, the singlet states $nsnp$ $^1P_1$ and $ns(n-1)d$ $^1D_2$ require further attention as the properties involving these states exhibit the largest deviations from other theoretical results. A similar pattern is observed in the other theoretical results as well. Based on our studies and careful analysis, the observed deviations of the two-valence properties may be attributed to the basis, V^{N-2} potential, we have used. We expect calculations with V^{N-1} potential basis could improve the results.

In conclusion, relativistic Fock-space coupled-cluster theory has theoretical and computational advantages for structure and properties calculations of two-valence systems. In this article we report the development of an all-particle two-valence relativistic Fock-space coupled-cluster theory and have demonstrated a scheme for properties calculations with the CC wave functions.

[1] F. Coester, Nucl. Phys. **7**, 421 (1958).

[2] F. Coester and H. Kümmel, Nucl. Phys. **17**, 477 (1960).

[3] G. Hagen, T. Papenbrock, D. J. Dean, and M. Hjorth-Jensen, Phys. Rev. Lett. **101**, 092502 (2008).

[4] H. S. Nataraj, B. K. Sahoo, B. P. Das, and D. Mukherjee, Phys. Rev. Lett. **101**, 033002 (2008).

[5] R. Pal, M. S. Safronova, W. R. Johnson, A. Derevianko, and S. G. Porsev, Phys. Rev. A **75**, 042515 (2007).

[6] T. A. Isaev, A. N. Petrov, N. S. Mosyagin, A. V. Titov, E. Eliav, and U. Kaldor, Phys. Rev. A **69**, 030501(R) (2004).

[7] R. F. Bishop, P. H. Y. Li, D. J. J. Farnell, and C. E. Campbell, Phys. Rev. B **79**, 174405 (2009).

[8] R. J. Bartlett and M. Musial, Rev. Mod. Phys. **79**, 291 (2007).

[9] R. F. Bishop, Theo. Chim. Acta **80**, 95 (1991).

[10] K. V. P. Latha, D. Angom, B. P. Das, and D. Mukherjee, Phys. Rev. Lett. **103**, 083001 (2009).

[11] L. W. Wansbeek, B. K. Sahoo, R. G. E. Timmermans, K. Jungmann, B. P. Das, and D. Mukherjee, Phys. Rev. A **78**, 050501(R) (2008).

[12] B. K. Sahoo, L. W. Wansbeek, K. Jungmann, and R. G. E. Timmermans, Phys. Rev. A **79**, 052512 (2009).

[13] C. Thierfelder and P. Schwerdtfeger, Phys. Rev. A **79**, 032512 (2009).

[14] B. K. Sahoo, B. P. Das, and D. Mukherjee, Phys. Rev. A **79**, 052511 (2009).

[15] D. Mukherjee, Pramana **12**, 203 (1979).

[16] I. Lindgren and J. Morrison, in *Atomic Many-Body Theory*, edited by G. Ecker, P. Lambropoulos, and H. Walther (Springer-Verlag, Berlin, 1985).

[17] B. K. Mani, K. V. P. Latha, and D. Angom, Phys. Rev. A **80**, 062505 (2009).

[18] B. K. Mani and D. Angom, Phys. Rev. A **81**, 042514 (2010).

[19] E. Eliav, U. Kaldor, and Y. Ishikawa, Phys. Rev. A **52**, 291 (1995).

[20] G. Hose and U. Kaldor, J. Phys. B **12**, 3827 (1979).

[21] G. D. Purvis and R. J. Bartlett, J. Chem. Phys. **76**, 1910 (1982).

[22] I. Lindgren, Phys. Rev. A **31**, 1273 (1985).

[23] A. Ynnerman, J. James, I. Lindgren, H. Persson, and S. Salomonson, Phys. Rev. A **50**, 4671 (1994).

[24] E. Eliav, U. Kaldor, and Y. Ishikawa, Phys. Rev. A **50**, 1121 (1994).

[25] S. Stellmer, M. K. Tey, B. Huang, R. Grimm, and F. Schreck, Phys. Rev. Lett. **103**, 200401 (2009).

[26] T. Akatsuka, M. Takamoto, and H. Katori, Nature Physics **4**, 954 (2008).

[27] A. D. Ludlow *et al.*, Science **319**, 1805 (2008).

[28] D. English, V. V. Yashchuk, and D. Budker, Phys. Rev. Lett. **104**, 253604 (2010).

[29] S. De, U. Dammalapati, K. Jungmann, and L. Willmann, Phys. Rev. A **79**, 041402(R) (2009).

[30] V. A. Dzuba and J. S. M. Ginges, Phys. Rev. A **73**, 032503 (2006).

[31] V. V. Flambaum, Phys. Rev. A **60**, R2611 (1999).

[32] K. Tsigutkin, D. Dounas-Frazer, A. Family, J. E. Stalnaker, V. V. Yashchuk, and D. Budker, Phys. Rev. Lett. **103**, 071601 (2009); Phys. Rev. A **81**, 032114 (2010).

[33] Y. B. Zeldovich, Sov. Phys. JETP **6**, 1184 (1958).

[34] Y. Takahashi *et al.*, in *Proceedings of CP Violation and its Origin*, edited by K. Hagiwara (KEK, Tukuba, 1997).

[35] V. Natarajan, Eur. Phys. J. D **32**, 33 (2005).

[36] Y. Takasu, K. Maki, K. Komori, T. Takano, K. Honda, M. Kumakura, T. Yabuzaki, and Y. Takahashi, Phys. Rev. Lett. **91**, 040404 (2003).

[37] Z. W. Barber, C. W. Hoyt, C. W. Oates, L. Hollberg, A. V. Taichenachev, and V. I. Yudin, Phys. Rev. Lett. **96**, 083002 (2006).

[38] G. P. Barwood, K. Gao, P. Gill, G. Huang, and H. A. Klein, Phys. Rev. A **67**, 013402 (2003).

[39] J. Stenger, H. Schnatz, C. Tamm, and H. R. Telle, Phys. Rev. Lett. **88**, 073601 (2002).

[40] E. Peik, B. Lipphardt, H. Schnatz, T. Schneider, C. Tamm, and S. G. Karshenboim, Phys. Rev. Lett. **93**, 170801 (2004).

[41] N. Fortson, Phys. Rev. Lett. **70**, 2383 (1993).

[42] I. Lindgren, J. Phys. B **7**, 2441 (1974).

[43] I. Lindgren, Phys. Scr. **32**, 291 (1985); **32**, 611 (1985).

[44] M. S. Safronova, W. R. Johnson, and U. I. Safronova, Phys. Rev. A **53**, 4036 (1996).

[45] H. C. Ho, W. R. Johnson, S. A. Blundell, and M. S. Safronova, Phys. Rev. A **74**, 022510 (2006).

[46] D. Mukherjee, R. K. Moitra, and A. Mukhopadhyay, Mol. Phys. **30**, 1861 (1975); **33**, 955 (1977).

[47] A. Mukhopadhyay, R. K. Moitra, and D. Mukherjee, J. Phys. B **12**, 1 (1979).

[48] I. Lindgren, Int. J. Quantum Chem. Symp. **12**, 33 (1978).

[49] D. Mukherjee, Chem. Phys. Lett. **125**, 207 (1986).

[50] B. Jeziorski and H. J. Monkhorst, Phys. Rev. A **24**, 1668 (1981).

[51] I. Lindgren and D. Mukherjee, Phys. Rep. **151**, 93 (1987).

[52] S. R. Hughes and U. Kaldor, Phys. Rev. A **47**, 4705 (1993).

[53] C. Schwartz, Phys. Rev. **97**, 380 (1955).

[54] A. K. Mohanty and E. Clementi, Chem. Phy. Lett. **157**, 348 (1989).

[55] R. K. Chaudhuri, P. K. Panda, and B. P. Das, Phys. Rev. A **59**, 1187 (1999).

[56] R. E. Stanton and S. Havriliak, J. Chem. Phys. **81**, 1910 (1984).

[57] W. R. Johnson, *Atomic Structure Theory: Lectures on Atomic Physics* (Springer-Verlag, Berlin, 2007).

[58] F. A. Parpia, C. Froese Fischer, and I. P. Grant, Comput. Phys. Commun. **94**, 249 (1996).

[59] P. Pulay, Chem. Phys. Lett. **73**, 393 (1980).

[60] N. Vaeck, M. Godefroid, and J. E. Hansen, Phys. Rev. A **38**, 2830 (1988).

[61] S. G. Porsev, M. G. Kozlov, Y. G. Rakhlina, and A. Derevianko, Phys. Rev. A **64**, 012508 (2001).

[62] I. M. Savukov and W. R. Johnson, Phys. Rev. A **65**, 042503 (2002).

[63] *NIST Atomic Spectroscopic Database* [http://physics.nist.gov/PhysRefData].

[64] E. Eliav, U. Koldor, and Y. Ishikawa, Phys. Rev. **53**, 3050 (1996).

[65] V. A. Dzuba, V. V. Flambaum, and M. G. Kozlov, Phys. Rev. A **54**, 3948 (1996).

[66] M. S. Safronova, M. G. Kozlov, W. R. Johnson, and D. Jiang, Phys. Rev. A **80**, 012516 (2009).

[67] S. G. Porsev, Y. G. Rakhlina, and M. G. Kozlov, J. Phys. B **32**, 1113 (1999).

[68] V. A. Dzuba and A. Dereviako, J. Phys. B **43**, 074011 (2010).

[69] N. J. Stone, At. Data Nucl. Data Tables **90**, 75 (2005).

[70] S. Salomonson and P. Öster, Phys. Rev. A **40**, 5559 (1989).

[71] A.-M. Martensson-Pendrill, D. S. Gough, and P. Hannaford, Phys. Rev. A **49**, 3351 (1994).

[72] W. M. Itano, Phys. Rev. A **73**, 022510 (2006).

[73] K. Krebs and H. Nelkowski, Z. Phys. **141**, 254 (1955).

[74] A.-M. Martensson-Pendrill, J. Phys. B **35**, 917 (2002).

[75] K.-Z. Yu, L.-J. Wu, B.-C. Gou, and T.-Y. Shi, Phys. Rev. A **70**, 012506 (2004).

[76] B. K. Sahoo, C. Sur, T. Beier, B. P. Das, R. K. Chaudhuri, and D. Mukherjee, Phys. Rev. A **75**, 042504 (2007).

[77] F. Buchinger *et al.*, Phys. Rev. C **41**, 2883 (1990).

[78] B. K. Sahoo, Phys. Rev. A **74**, 020501(R) (2006).

[79] P. Villemoes, A. Arnesen, F. Heijkenskjold, and A. Wannstrom, J. Phys. B **26**, 4289 (1993).

[80] R. E. Silverans, G. Borghs, P. De Bisschop, and M. Van Hove, Phys. Rev. A **33**, 2117 (1986).

[81] R. E. Silverans, G. Borghs, G. Dumont, and J. M. Van den Cruyce, Z. Phys. **295**, 311 (1980).

[82] M. Van. Hove, Ph.D thesis, University of Cambridge, UK, 1974.

[83] R. W. Berends and L. Maleki, J. Opt. Soc. Am. B **9**, 332 (1992).

[84] M. G. Kozlov and S. G. Porsev, Eur. Phys. J. D **5**, 59 (1999).

[85] M. Gustavsson, G. Olson, and A. Rosen, Z. Phys. A **290**, 231 (1979).

[86] S. G. Schmelling, Phys. Rev. A **9**, 1097 (1974).

[87] G. zu. Putliz, Ann. Phys. **11**, 248 (1963).

[88] H.-J. Kluge and H. Z. Sauter, Z. Phys. **270**, 295 (1974).

[89] W.-G. Jin *et al.*, J. Phys. Soc. Jpn. **60**, 2896 (1991).

[90] B. Budick and J. Snir, Phys. Rev. **178**, 18 (1969).

[91] O. Topper, G. H. Guthohrlein, and P. Hillermann, in *Proceedings 29th Conference of the European Group for Atomic Spectroscopy (EGAS)*, Abstract, 233 (1997).

[92] S. M. Heider and G. O. Brink, Phys. Rev. A **16**, 1371 (1977).

[93] C. Guet and W. R. Johnson, Phys. Rev. A **44**, 1531 (1991).

[94] V. A. Dzuba, V. V. Flambaum, and J. S. M. Ginges, Phys. Rev. A **63**, 062101 (2001).

[95] U. I. Safronova and M. S. Safronova, Phys. Rev. A **79**, 022512 (2009).

[96] S. G. Porsev, Y. G. Rakhlina, and M. G. Kozlov, Phys. Rev. A **60**, 2781 (1999).

[97] J. Migdalek and W. E. Baylis, J. Phys. B **24**, L99 (1991).

[98] M. D. Kunisz, Acta Phys. Polon. A **62**, 285 (1982).